A COMPUTATIONAL AND GEOMETRIC APPROACH TO PHASE RESETTING CURVES AND SURFACES

ANTONI GUILLAMON AND GEMMA HUGUET

Abstract. This work arises from the purpose of relating time problems in biological systems with some known tools in dynamical systems. More precisely, how are the phase resetting curves (PRCs) around a limit cycle γ of a vector field X related to the fact that X is the infinitesimal generator of a Lie symmetry ($[Y, X] = \mu Y$). We show how the time variables involved in the Lie symmetry provide a natural way (a kind of *normal form*) to express the vector field around γ, similar to action-angle variables for integrable systems. In addition, the knowledge of the orbits of Y gives a trivial way to compute the PRC, not only on γ, but also in a neighborhood of it, thus obtaining what we call *phase resetting surfaces* (PRSs). However, the aim of the paper is not only to state relationships among different concepts, but also to perform the effective computation of these symmetries. The numerical scheme is based on the theoretical ground of the so-called parameterization method to compute invariant manifolds (the orbits of Y) in a neighborhood of γ. Limit cycles in biological (more specifically, neuroscience) models encompass numerical problems that are often neglected or underestimated; we present a discussion about them and give general solutions whenever it is possible. Finally, we use all theoretical and numerical results to compute both the PRCs and PRSs and the isochronous sections of limit cycles for well-known biological models. In this part of the paper, we also explore how the PRCs evolve (in the parameter space) between different bifurcation values.

1. Introduction

The behavior of coupled oscillators in biology and, more intensively, in neuroscience has been the subject of a great deal of recent interest and there is a wide literature on this topic (see [Izh07] for a survey), mainly because many oscillators can be described by their phase variable. Moreover, under generic conditions, the phase of the oscillation can be also defined outside the hyperbolic limit cycle via asymptotic phase. Thus, the stable manifold of a point x_0 on a limit cycle is the union of points having equal phases, and it is often referred to as the isochron of x_0.

To study synchronization, a useful measurable property of a neural oscillator is its phase resetting curve (PRC). The PRC is found by perturbing the oscillation with a brief stimulus at different times on its cycle and measuring the resulting phase-shift from the unperturbed system. It is a very useful tool to explain how the coupling between neurons can affect the phase and lead them to a synchronized or non-synchronized activity.

Phase resetting curves (PRCs) constitute a powerful resource in time-control problems in biological processes. For instance, in the study of circadian rhythms, phase resetting curves are indicators for the experimentalists to know the peaks of the phase advancement and for the practitioners to administrate drugs (see for instance [CKWJ03], [DN94] or [PZG07] for different contexts); that is, to know the optimal phase advancement.

2000 *Mathematics Subject Classification.* 34C14, 34C20, 92-08; 37N25, 92B05.

Different methods are known to compute the PRCs, see [Izh07, Ch. 10] for a survey. One of the most effective is the so-called *adjoint method*, see [EK91] (also [BHM04] for a review). Recently, Govaerts and Sautois (see [GS06]) have developed a new algorithm to solve the adjoint method problem accompanied with the implementation of continuation methods to study PRCs along families of vector fields with a persistent limit cycle.

Typically, solutions to the models of interest tend asymptotically to a limit cycle. However, one may be interested in computing the phase advancement in the transient state, when the dynamics has not relaxed back to the limit cycle. This occurs when the period of stimulation is too short and is favored by factors like a slow attraction to the limit cycle, a large stimulus amplitude, other external stimuli, random fluctuations, bursting-like stimuli, ... Thus, the study of the phase advancement under a certain stimulus in a *neighborhood of the limit cycle*, not only *on the limit cycle*, is also interesting.

Since the method that we develop in this manuscript gives a "natural" parameterization of an entire neighborhood of a limit cycle, and the way we obtain the phase resetting curves is independent on whether a point is on the limit cycle or not, we can extend the computation of the phase resetting curves to a neighborhood and obtain what we call *phase resetting surfaces* (PRS from now on); that is, we can evaluate the phase advancement even when the stimulus is performed out of the limit cycle. The restriction of our method to the limit cycle gives the numerical scheme also used in [GS06].

In the examples, we also include a discussion on the relationship between the excitability types and the types of the corresponding PRCs. This issue was introduced by Ermentrout in [Erm96]; models with strictly positive or mainly positive PRC are called usually "Type 1 PRC" or "Class 1", whereas models whose PRC changes sign and present a negative regime (delay in the phase) are known as "Type 2 PRC" or "Class 2". The PRC type have effects on the synchronization of an oscillator with a periodic pulse train. For instance, for Type 1 models, that is with a PRC mostly positive, they easily synchronize with fast inputs but they cannot synchronize with slower inputs. This is because they can advance the phase to catch up with faster inputs but they cannot delay the phase. This is not the case for Type 2 models because they can advance or delay the phase. We study, in parametric families, the evolution from one type to another. It can be observed how the negative parts of the PRC for a "Type 2 PRC" oscillator shrink as some bifurcation parameter evolves until it almost vanishes near to a "Type 1 excitability" value (that is, close to a frequency zero limit cycle bifurcation), corresponding also to a "Type I PRC" value, see Example 9.2 and (40) ($I_{app} = 10$). We are more concerned with the observation and biological consequences of these changes between PRCs inside a family of vector fields, rather than carrying out a systematic computation of PRCs with respect to some parameter. As mentioned above, this job has been done in [GS06].

In the examples we also show (see Figs. 2 to 6) that, depending on the geometry of the isochrons, the shape of the phase resetting surface may be different from the shape of the phase resetting curve in such a way that systems with "Type I PRC" can present regions with negative PRS, thus allowing, away from the limit cycle, a delay of the phase which is not supposed for "Type I PRC" oscillators.

The mathematical formalism that we use to obtain information about isochrons, PRCs and PRSs is based on Lie symmetries, see [Sab05] or [FGG07] for new applications to limit cycles. Indeed, given a vector field X with a limit cycle γ, it is proved the equivalence between the existence of a Lie symmetry $[Y, X] = \mu Y$ and the foliation of a neighborhood of γ by isochrons (that is, with asymptotic phase well defined). Parallel, to this theory, Cabré-Fontich-de la Llave have developed

a method to parameterize invariant manifolds around an invariant object, see for instance [CFL05] for the part related to limit cycles. This so-called *parameterization method* is much easier to implement than the computation of Lie symmetries. In this paper we relate the two approaches; in fact, we prove that the coordinate curves of the parameterization are exactly the orbits of the unknown vector field Y.

The paper is organized as follows: in Section 2 we give the necessary background (on isochronous sections, Lie symmetries, parameterization method and phase resetting curves) to tackle the rest of the paper. In Section 3, we relate the Lie symmetries with the parameterization method. Sections 4 and 6 are devoted to develop the effective method to compute the isochrons and the phase resetting curves (and surfaces), using the parameterization method. For the purpose of comparison, in Section 5, we explain the adjoint method and prove that our result is also a solution of the adjoint equation. In Section 7, we take care of the details of the numerical implementation of the method, an aspect which is often overlooked although it is not trivial for slow-fast systems. We devote Section 8 to envision the application of our method to higher dimensions. We end the paper with some examples, in Section 9, and a final discussion (Section 10).

2. Background and statement of the problem

In this section we go through the background about the main tools that will be related later on. In general, these tools are defined for vector fields in $\mathbb{R}^d$, although for the purposes of this paper we will restrict to $d = 2$ from Section 3 on.

2.1. Isochronous sections of a limit cycle.

Let us consider an autonomous system of ODEs

$$\dot{x} = X(x), \quad x \in U \subseteq \mathbb{R}^d, \quad d \geq 2, \tag{1}$$

having a periodic orbit γ of period T, parameterized by $\theta = t/T$ as

$$\begin{aligned} \gamma \colon \mathbb{T} = \mathbb{R}/\mathbb{Z} &\longrightarrow \mathbb{R}^d \\ \theta &\longrightarrow \gamma(\theta) \end{aligned} \tag{2}$$

in order to have period 1, that is $\gamma(\theta) = \gamma(\theta + 1)$.

For the numerical purposes of this paper we will assume that X is an analytic vector field and so, all the functions and manifolds that we will associate to it. Nevertheless, the theoretical background that we are quoting in this section is still valid for lower regularity vector fields.

Definition 2.1. *We say that a point $q \in \Omega \subset \mathbb{R}^d$, where Ω is an open domain containing the limit cycle γ, is in* asymptotic phase *with a point $p \in \gamma$ if*

$$\lim_{t \to +\infty} |\Phi_t(q) - \Phi_t(p)| = 0, \text{ or}$$

$$\lim_{t \to -\infty} |\Phi_t(q) - \Phi_t(p)| = 0,$$

where Φ_t is the flow associated to the vector field X.

The set of points having the same asymptotic phase is called isochron.

Definition 2.2. *We will say that a limit cycle γ is isochronous if there exists an open neighborhood Ω containing γ such that every point in Ω is in phase with a point on γ.*

Remark 2.3. *Notice that the isochrons are mapped to isochrons by the flow Φ_t of the vector field X. Hence, they are Φ_T-invariant, that is $\Phi_T(q)$ belongs to the isochron of q.*

This extends the notion of phase of oscillation to a neighborhood in the basin of attraction of the limit cycle. Hence, in a neighborhood Ω of the limit cycle γ there exists a unique scalar function

$$\begin{array}{rcl} \vartheta\colon \Omega \subset \mathbb{R}^d & \longrightarrow & \mathbb{T} = [0,1) \\ x & \longmapsto & \vartheta(x) \end{array} \tag{3}$$

such that

$$\lim_{t\to+\infty(-\infty)} |\Phi_t(x) - \gamma(t + T\vartheta(x))| = 0.$$

The value $\vartheta(x)$ is the asymptotic phase of x and the isochrons are the level sets of $\vartheta(x)$, since it is constant on each isochron.

2.2. **Isochrons, stable manifolds and Lie symmetries.** From a seminal paper by Winfree ([Win75]) and the theoretical answers given by Guckenheimer in a subsequent paper ([Guc75]), it is known that phase sets or isochrons and stable manifolds of hyperbolic limit cycles have a common link: if the limit cycle is stable, then the isochrons are the leaves of the stable manifold, that is $W^s(\gamma(\theta))$, for $\theta \in \mathbb{T}$.

Remark 2.4. *Notice that the case of a hyperbolic unstable limit cycle is equivalent to the stable case just reversing the time. However, when one works in dissipative systems it only makes sense to talk about attractors because the other invariant objects cannot be seen when one integrates forward the system. Hence, from now on, we will only mention the stable case.*

Not much is said about the computation of these isochrons probably perhaps they can often be reduced to the computation of stable manifolds, which have been thoroughly studied.

New papers recovering the problem of the existence of isochrons for a generic non-hyperbolic limit cycle in the plane have appeared recently ([CL04, Sab05]). From Chicone and Liu's work, [CL04], we know that a limit cycle γ of a $\mathcal{C}^2$ planar vector field is isochronous if and only if it is hyperbolic or it is a non-hyperbolic limit cycle satisfying $\pi''(p) \neq 0$ and $\tau'(p) = 0$, where τ is the time of the first return to a Poincaré section Σ at $p \in \gamma$ and π is the corresponding Poincaré map. Moreover, in [Sab05], Sabatini proves that a limit cycle γ of a $\mathcal{C}^2$ planar vector field X is isochronous if and only if the vector field X is an infinitesimal generator of another C^2 planar vector field Y transversal to X; that is, if

$$[Y, X] = \mu\, Y, \tag{4}$$

for some C^2 function $\mu\colon \mathbb{R}^2 \longrightarrow \mathbb{R}$, where $[\,,\,]$ stands for the Lie bracket of the two vector fields. Moreover, it is stated that, in this case, the orbits of Y crossing the limit cycle γ are its isochrons because, by the Lie symmetry, the flow of X sends orbits of Y to orbits of Y.

Finally, Freire et al., see [FGG07], give a closed formula for the characteristic exponent of a limit cycle γ of a planar $\mathcal{C}^1$ vector field X in terms of μ in (4). More precisely, they prove that the characteristic exponent of γ is given by

$$\lambda = \int_0^T \mu(\gamma(t/T))dt. \tag{5}$$

Although the result of Sabatini is a nice geometrical characterization of isochronous limit cycles, the difficulty arises when trying to find μ and Y. In this paper, we link this result with the parameterization method developed in [CFL05] to compute the two-dimensional stable manifold containing γ, and we implement it numerically to obtain local expansions of μ and Y.

2.3. **The parameterization method.** In this subsection we introduce the parameterization method described in [CFL05]. For limit cycles in planar systems, it consists of looking for a parameterization of the two-dimensional stable manifold in terms of the phase variable θ on the limit cycle and another variable σ which moves along the isochron/leave of the stable manifold and corresponds to the time of the orbits of the vector field Y in (4). Hence, we will be looking for a map

$$\begin{aligned} K\colon \mathbb{T}\times U \subset \mathbb{T}\times\mathbb{R} &\longrightarrow \mathbb{R}^2 \\ (\theta,\sigma) &\longmapsto K(\theta,\sigma), \end{aligned} \tag{6}$$

where U is an open interval containing 0, and a scalar λ such that they satisfy the equation

$$\left(\frac{1}{T}\frac{\partial}{\partial\theta} + \frac{\lambda\sigma}{T}\frac{\partial}{\partial\sigma}\right) K(\theta,\sigma) = X(K(\theta,\sigma)), \tag{7}$$

where T is the period of the limit cycle.

On the computational side, in [CFL05], the authors provide a method to solve the invariance equation (7) that leads immediately to practical numerical algorithms. We have implemented it in several biological models (specially from neuroscience) in which the control of the phase advancements becomes crucial. In Section 6 we review the method and the algorithms to solve equation (7) and in Section 7 we discuss the numerical implementation. Similar implementations of this method have been performed in [HL06] for the computation of stable and unstable manifolds of invariant tori in quasi-periodic maps.

2.4. **Phase response curves and surfaces.** As mentioned in the Introduction, phase resetting curves are a key tool to study phase advancement in oscillators. Here we introduce the basic background.

Let us consider an oscillator of the form (1) with a stable limit cycle γ of period T (let us say, for instance, a periodically spiking neuron) which is stimulated at a phase $\theta = t_s/T$ with an arbitrary perturbation.

The effect of the perturbation is to produce a phase shift that can be an advance or a delay depending on the time of the stimulus t_s relative to the phase of the oscillation θ, leading to a change of the period. The representation of this phase shift is usually called *Phase Response Curve* or *Phase Resetting Curve* (PRC). They are typically defined as

$$\Delta\vartheta = (T - T_{new})/T \tag{8}$$

where T_{new} is the period for the perturbed limit cycle.

In this paper we will focus on the particular case of infinitesimally small perturbations in duration and amplitude. In this case, the perturbation consists of a pulse that instantaneously displaces the trajectory away from the limit cycle in a certain direction by a certain amplitude. Mathematically, we consider

$$\dot{x} = X(x) + \epsilon\delta(t - t_s) \tag{9}$$

where $\epsilon = (\epsilon_1, \ldots, \epsilon_d) \in \mathbb{R}^d$ and $\delta(t)$ is the Dirac delta function.

When $|\epsilon| \ll 1$, it is common in the theory of weakly coupled neural oscillators (Ermentrout and Kopell, 1990) to construct the so called *infinitesimal Phase Resetting Curve* (iPRC). Using the scalar function ϑ given in (3) that associates to every point in a neighborhood of the limit cycle a phase in $[0, 1)$, it is easy to see that the iPRC for an instantaneous perturbation as in (9) is mathematically equivalent to

$$\Delta\vartheta(x) = \epsilon \cdot \nabla\vartheta(x) = \left(\frac{\partial\vartheta}{\partial x_1}(x), \ldots, \frac{\partial\vartheta}{\partial x_d}(x)\right)$$

for $x \in \gamma$, see [Izh07, Ch. 10] for the details.

Note that the pulse in (9) can be in any direction in $\mathbb{R}^d$. Usually, one studies the PRCs for the directions given by a vector basis of $\mathbb{R}^d$. For instance, for the planar case ($d = 2$), we will consider the PRCs corresponding to $\epsilon = (1, 0)$ and $\epsilon = (0, 1)$ and we will refer to them as PRC_1 and PRC_2, respectively. For models in neuroscience, one is usually interested only on the PRC for perturbations in the direction of the voltage, that is, $\partial\vartheta(x)/\partial V$, for $x \in \gamma$.

Although in the literature the phase shift is only computed on the limit cycle, that is $x \in \gamma$, the isochrons allow to naturally extend it in a neighborhood of the limit cycle and introduce a new concept that we call *Phase Resetting Surface* (also PRS from now on). In general, PRS are not considered in the literature because the methods to obtain the PRCs are not easily extendable.

The phase resetting surface tabulates the change in the phase produced by a perturbation as a function of the phase θ and the distance σ to the limit cycle computed on the isochron at which it is received. Notice that the PRC is just the section $\sigma = 0$ of the PRS. Hence, PRSs are a generalization of the PRCs for $\sigma \neq 0$. This tool can be very useful if we want to stimulate the oscillator repeatedly, without needing to wait for the oscillator to relax back to the limit cycle attractor. This required time to relax back is specially inconvenient when the attraction to the limit cycle is too slow or the amplitude of the stimulus is too large.

The classical method for computing PRCs was given by Ermentrout and Kopell in [EK91] and is commonly known as the *Adjoint method*. In Section 4 we describe a new alternative method that allows to compute not only the PRC but also the PRS, using the Lie symmetries formalism and the numerical scheme provided by the parameterization method.

3. Lie symmetries and normal forms around limit cycles

In this section we establish a relation between the existence of a Lie symmetry and a 2-dimensional invariant manifold parameterized by the phase θ and the variable σ for the limit cycle of a planar vector field. The main result is given by Theorem 3.1.

Theorem 3.1. *Let γ be a hyperbolic T-periodic orbit of a planar analytic vector field X parameterized by θ according to* (2)*. Then, there exists a transversal vector field Y and a scalar function μ, both analytic, such that in a neighborhood Ω of the periodic orbit γ*

$$[Y, X] = \mu Y,$$

if and only if there exists a manifold $\mathcal{M}$ which is invariant under the flow of X and can be parameterized by an analytic map $K\colon \mathbb{T} \times U \subset \mathbb{R} \to \mathbb{R}^2$, satisfying

$$\left(\frac{1}{T}\partial_\theta + \left(\int_0^\sigma \mu(K(\theta,\tau))d\tau\right)\partial_\sigma\right) K(\theta,\sigma) = X \circ K(\theta,\sigma). \tag{10}$$

Moreover, $Y \circ K = \partial_\sigma K$, or equivalently

$$K(\theta,\sigma) = \psi_\sigma(\gamma(\theta)), \tag{11}$$

where ψ_σ is the flow of the vector field Y.

Proof: Let us look at the first implication. Let us consider $K(\theta,\sigma) = \psi_\sigma(\gamma(\theta))$, where ψ_σ is the flow associated to the vector field Y and $\gamma(\theta)$ is the parameterization of the periodic orbit of the vector field X.

Then, notice that

$$\partial_\sigma(X \circ K(\theta,\sigma)) = DX \circ K(\theta,\sigma)\partial_\sigma K(\theta,\sigma) = (DX \circ K(\theta,\sigma))(Y \circ K(\theta,\sigma)).$$

Using the Lie symmetry $DXY - DYX = \mu Y$, we have

$$\frac{\partial}{\partial\sigma} X \circ K(\theta,\sigma) = (DY \circ K(\theta,\sigma))(X \circ K(\theta,\sigma)) + \mu(K(\theta,\sigma))(Y \circ K(\theta,\sigma)). \tag{12}$$

Hence, $X \circ K(\theta,\sigma)$ is a solution of the linear equation (12) with initial condition

$$X \circ K(\theta,0) = \gamma(\theta). \tag{13}$$

Let Ψ_σ be the fundamental solution of the homogeneous equation

$$\frac{\partial}{\partial\sigma} X \circ K(\theta,\sigma) = (DY \circ K(\theta,\sigma))(X \circ K(\theta,\sigma)), \tag{14}$$

then, the variation of parameters formula tells us that the solution of (12) with initial condition (13) is given by

$$X \circ K(\theta,s) = \Psi_\sigma X(\gamma(\theta)) + \Psi_\sigma \int_0^\sigma \Psi_s^{-1} \mu(K(\theta,s))(Y \circ K(\theta,s)) ds.$$

Notice that $\Psi_s^{-1} Y(K(\theta,s))$ is independent of s, that is

$$\begin{aligned}
\partial_s(\Psi_s^{-1} Y(K(\theta,s))) &= -\Psi_s^{-1}(DY \circ K(\theta,s))\Psi_s\Psi_s^{-1}(Y \circ K(\theta,s)) \\
&\quad + \Psi_s^{-1}(DY \circ K(\theta,s))(Y \circ K(\theta,s)) \\
&= -\Psi_s^{-1}(DY \circ K(\theta,s))(Y \circ K(\theta,s)) \\
&\quad + \Psi_s^{-1}(DY \circ K(\theta,s))(Y \circ K(\theta,s)) \\
&= 0
\end{aligned}$$

then we can take $\Psi_s^{-1} Y(K(\theta,s)) = \Psi_\sigma^{-1} Y(K(\theta,\sigma))$ and we are led with the following expression for $X \circ K(\theta,\sigma)$,

$$X \circ K(\theta,\sigma) = \Psi_\sigma X(\gamma(\theta)) + \Psi_\sigma \Psi_\sigma^{-1} Y(K(\theta,\sigma)) \int_0^\sigma \mu(K(\theta,s)) ds.$$

Finally, using that the parameterization K is given by the orbits of the vector field Y on the limit cycle γ, see equation (11), we have

$$\partial_\theta K(\theta,\sigma) = \partial_\theta \psi_\sigma(\gamma(\theta)) = D\psi_\sigma(\gamma(\theta)) T X(\gamma(\theta)) = T\Psi_\sigma X(\gamma(\theta)),$$

and the expression for $X \circ K(\theta,\sigma)$ reads out

$$X \circ K(\theta,\sigma) = \left(\frac{1}{T}\partial_\theta + \left(\int_0^\sigma \mu(K(\theta,\tau)) d\tau \right) \partial_\sigma \right) K(\theta,\sigma),$$

as we wanted to see.

The implication the other way follows in the following way. Let K being a parameterization of the stable manifold $\mathcal{M}$ satisfying equation (10). Consider Y the vector field whose orbits for the points on the limit cycle $\gamma(\theta)$ are given by $\{K(\theta,\sigma) | \sigma \in \mathbb{R}\}$. Let σ be the integration time along the orbits of the vector field Y. Therefore,

$$Y \circ K(\theta,\sigma) = \partial_\sigma K(\theta,\sigma). \tag{15}$$

The fact that the curves $\{K(\theta_0,\sigma) | \sigma \in \mathbb{R}\}$ are transversal to the orbits of X implies also that Y is transversal to X.

We next prove that X is a normalizer of the vector field Y. From equation (10), taking derivatives with respect to σ, we get

$$\left(\frac{1}{T}\partial_\theta + \left(\int_0^\sigma \mu(K(\theta,\tau)) d\tau \right) \partial_\sigma \right) \partial_\sigma K + (\mu \circ K)\partial_\sigma K = (DX \circ K)\partial_\sigma K,$$

and using (15), we get

$$\left(\frac{1}{T}\partial_\theta + \left(\int_0^\sigma \mu(K(\theta,\tau))d\tau\right)\partial_\sigma\right)(Y\circ K) + (\mu\circ K)(Y\circ K) = (DX\circ K)(Y\circ K).$$

By the chain rule,

$$(DY\circ K)\left(\frac{1}{T}\partial_\theta + \left(\int_0^\sigma \mu(K(\theta,\tau))d\tau\right)\partial_\sigma\right)K + (\mu\circ K)(Y\circ K) = (DX\circ K)(Y\circ K),$$

and again, by the invariance equation (10), we obtain

$$\begin{aligned}(DX\circ K)(Y\circ K) - (DY\circ K)(X\circ K) &= (\mu\circ K)(Y\circ K)\\ [Y,X] &= \mu Y,\end{aligned}$$

as we wanted to prove. □

3.1. **Simplifying the invariance equation** (10)**.** We would like to remark that there is a certain freedom for the choice of Y and μ. Thus, given a vector field Y and a scalar function μ such that $[Y,X] = \mu Y$, then for a non-vanishing smooth scalar function f it turns out that

$$[f\,Y, X] = \left(\mu - \frac{\nabla f^T X}{f}\right)(f\,Y)\,.$$

Using this freedom, it will be convenient to choose μ to be constant. From (5) we know that the characteristic exponent for the periodic orbit is given by

$$\lambda = \int_0^T \mu dt = \mu T.$$

Then, it is natural to choose $\mu = \lambda/T$, where λ is the characteristic exponent of the periodic orbit γ.

Hence, the invariance equation for the parameterization of the invariant manifold $\mathcal{M}$ is given by (7), that we recall here

$$\left(\frac{1}{T}\partial_\theta + \frac{\lambda\sigma}{T}\partial_\sigma\right)K(\theta,\sigma) = X\circ K(\theta,\sigma).$$

From equation (7) it is clear that $\mathcal{M} := \mathit{Range}(K)$ is an invariant manifold for the flow of X. Moreover, the motion generated by the vector field X on $\mathcal{M}$ expressed in the variables (θ,σ) parameterizing $\mathcal{M}$, is given by

$$\begin{aligned}\dot\theta &= 1/T,\\ \dot\sigma &= \lambda\sigma/T.\end{aligned} \tag{16}$$

That is, the variable θ rotates at a constant speed $1/T$ and the variable σ moves exponentially. Hence,

$$\Phi_t(K(\theta_0,\sigma_0)) = K(\theta_0 + t/T, \sigma_0 e^{\lambda t/T}),$$

where Φ_t is the flow of the vector field X.

Therefore the orbit of a point $K(\theta_0,\sigma)$, for any $\sigma\in\Omega$, approaches exponentially fast to the orbit of the point $K(\theta_0,0)$, which corresponds to the point $\gamma(\theta_0)$ on the limit cycle. Hence,

$$\{K(\theta_0,\sigma)\,|\,\sigma\in\Omega\}\subset W^s_{\gamma(\theta_0)},$$

that is, the point $K(\theta_0,\sigma)$ is contained in the isochron of $\gamma(\theta_0)$. Moreover $W^s_\gamma = \bigcup_{\theta\in[0,1)} W^s_{\gamma(\theta)}$.

Since, in this particular case the invariant stable manifold for the periodic orbit γ is 2-dimensional in $\mathbb{R}^2$, the parameterization in terms of the phase variable θ that gives the position on the limit cycle and σ, which is a variable that moves along a

transversal direction and corresponds to the integration time along the orbits of the vector field Y, is also a parameterization of the phase space $\mathbb{R}^2$ in a neighborhood of the limit cycle. The expression of the vector field X in the variables (θ, σ) can be considered as the normal form for a planar vector field around a limit cycle, reminiscent of the action-angle variables for conservative systems.

4. Computation of Phase Resetting Curves and Surfaces

The parameterization K and the vector field Y jointly with the characteristic exponent λ allow us to compute the *isochrons* and the *Phase Resetting Curves and Surfaces* (PRS).

4.1. **Computing the Isochrons.** We already mentioned that the orbit of the points given by $K(\theta_0, \sigma)$, for any $\sigma \in U$ approach exponentially fast the orbit of the point $K(\theta_0, 0) = \gamma(\theta_0)$.

Therefore a parameterization of the isochron of the point $\gamma(\theta_0)$ is given by the analytic map

$$\begin{array}{rccc} K(\theta_0, \cdot)\colon U \subset \mathbb{R} & \longrightarrow & \mathbb{R}^2 \\ \sigma & \longmapsto & K(\theta_0, \sigma). \end{array}$$

4.2. **Computing the PRS.** We already mentioned in Section 2.4 that from the mathematical point of view, the change of phase due to a pulse stimulation at a point $p = K(\theta, \sigma)$ in a neighborhood Ω of the limit cycle γ is given by

$$\nabla\vartheta(p) = \left(\frac{\partial\vartheta}{\partial x}(p), \frac{\partial\vartheta}{\partial y}(p)\right).$$

In order to compute $\nabla\vartheta(p)$ we consider the following argument: on the one hand, the isochrons are given by the level sets of the function $\vartheta\colon \mathbb{R}^2 \to \mathbb{R}$, introduced in (3), which associates a phase to each point in a neighborhood of the limit cycle. On the other hand, they are the orbits of a vector field Y satisfying (4). Hence, it is clear that $\nabla\vartheta(p)$ has the same direction as $Y^{\perp}(p)$, which corresponds to the vector orthogonal to Y on p given by

$$Y(p) = Y(K(\theta, \sigma)) = \partial_\sigma K(\theta, \sigma).$$

We only need to add some normalization. Notice that for a trajectory $\phi_t(p)$, $p \in \Omega$ where ϕ_t is the flow of the vector field X, we have

$$\frac{d\vartheta}{dt}(\phi_t(p)) = 1/T,$$

therefore

$$\frac{d\vartheta}{dt}(\phi_t(p)) = \nabla\vartheta(\phi_t(p)) \cdot \frac{d}{dt}\phi_t(p) = \nabla\vartheta(\phi_t(p)) \cdot X(\phi_t(p)) = 1/T.$$

Using this normalization we have that for any $p \in \Omega$, the PRC is given by

$$\nabla\vartheta(p) = \frac{Y^{\perp}(p)}{T < Y^{\perp}(p), X(p) >}, \tag{17}$$

where $<,>$ denotes the dot product.

The PRC is just the PRS restricted to the points on the limit cycle, that is $\sigma = 0$, then for $p = K(\theta, 0) \in \gamma$

$$\nabla\vartheta(K(\theta, 0)) = \frac{Y^{\perp}(K(\theta, 0))}{T < Y^{\perp}(K(\theta, 0)), X(K(\theta, 0)) >},$$

where $K(\theta,0)=K_0(\theta)=\gamma(\theta)$ and $Y(K(\theta,0))$ is given by

$$Y(K(\theta,0))=\partial_\sigma K(\theta,0)=K_1(\theta).$$

Therefore,

$$\nabla\vartheta(\gamma(\theta))=\frac{K_1^\perp(\theta)}{<K_1^\perp(\theta),X(\gamma(\theta))>}\,. \tag{18}$$

5. The relation with the Adjoint method

As we already mentioned in the introduction, the reference method in neuroscience which is commonly used to compute Phase Resetting Curves, is the *Adjoint Method* (see [EK91], Hoppenstead). It essentially computes the gradient of the asymptotic phase at the points $p\in\gamma$, that is $\nabla\vartheta(p)$, by looking for a T-periodic solution of the equation

$$\frac{d\nabla\vartheta(\gamma(t/T))}{dt}=-DX^T(\gamma(t/T))\nabla\vartheta(\gamma(t/T)), \tag{19}$$

where $DX^T(\gamma(t/T))$ is the transpose of the real matrix $DX(\gamma(t/T))$, with the condition

$$\nabla\vartheta(\gamma(t/T))\cdot X(\gamma(t/T))=\frac{1}{T}\,,$$

which in particular must hold for $t=0$.

This procedure has been automated in the program *XPPAUT*, see [Erm02].

However, the Adjoint problem can be extended to a neighborhood of the limit cycle. The idea of this generalization is summarized in the following Proposition:

Proposition 5.1. *Let γ be a hyperbolic T-periodic orbit of a planar analytic vector field X parameterized by θ according to* (2)*. Assume that there exists a transversal vector field Y satisfying* (4) *in a neighborhood Ω. Then, given a trajectory $\phi_t(p)$, $p\in\Omega$ we have that*

$$\nabla\vartheta(\phi_t(p))=\frac{Y^\perp(\phi_t(p))}{T<Y^\perp(\phi_t(p)),X(\phi_t(p))>} \tag{20}$$

solves the Adjoint Problem

$$\frac{d\nabla\vartheta(\phi_t(p))}{dt}=-DX^T(\phi_t(p))\nabla\vartheta(\phi_t(p)), \tag{21}$$

with the condition

$$\nabla\vartheta(\phi_t(p))\cdot X(\phi_t(p))=\frac{1}{T}\,. \tag{22}$$

Proof: Notice first that, by construction, condition (22) is clearly satisfied.

Let us prove then that (20) is a solution of (21). In order to check this statement, we first introduce the matrix J given by

$$J=\begin{pmatrix}0&-1\\1&0\end{pmatrix} \tag{23}$$

such that $Y^\perp=JY$. Notice that for a 2×2 real matrix A we have

$$(JA)-(JA)^T=\mathrm{tr}(A)J. \tag{24}$$

Now, we consider the derivative of $\vartheta(\phi_t(p))$ with respect to the time. In order to simplify notation we set $x=\phi_t(p)$, $g(x):=<Y^\perp(x),X(x)>$ and $\tau(x)=\mathrm{tr}(DX)(x)$.

Using that $\frac{d}{dt}Y(\phi_t(p)) = DY(\phi_t(p))X(\phi_t(p))$, we have

$$\begin{aligned}\frac{d}{dt}\nabla\vartheta(x) =& \frac{J\,DY(x)\,X(x)}{T\,g(x)} \\ & - \frac{Y^{\perp}(x)\,(< JDY(x)X(x), X(x) > + < JY, DX(x)\,X(x) >)}{T\,g(x)^2}.\end{aligned}$$

Using now that the Lie symmetry gives $DX\,Y - DY\,X = \mu Y$, that expression (20) reads out as $\nabla\vartheta(x) = (J\,Y(x))/(T\,g(x))$ and dot product properties (namely,

$$< JY(x), DX(x)\,X(x) >=< DX(x)^T\,JY(x), X(x) >),$$

we obtain

$$\begin{aligned}\frac{d}{dt}\nabla\vartheta(x) =& \frac{J\,DX(x)\,Y(x) - \mu(x)\,JY(x)}{T\,g(x)} \\ & - \frac{\nabla\vartheta(x)\left(< JDX(x)Y(x) - \mu(x)\,JY(x) + DX(x)^T\,JY(x), X(x) >\right)}{g(x)}.\end{aligned}$$

Applying equation (24) and $(J\,DX(x))^T = -DX(x)^T\,J$, we are led to

$$\begin{aligned}\frac{d}{dt}\nabla\vartheta(x) =& \frac{(-DX(x)^T + \tau(x) - \mu(x))JY(x)}{T\,g(x)} \\ & - \frac{\nabla\vartheta(x)\,(< (\tau(x) - \mu(x))JY(x), X(x) >)}{g(x)}.\end{aligned}$$

In fact, again since $\nabla\vartheta(x) = (J\,Y(x))/(T\,g(x))$, it can be written as:

$$\begin{aligned}\frac{d}{dt}\nabla\vartheta(x) =& (-DX(x)^T + \tau(x) - \mu(x))\nabla\vartheta(x) \\ & - T\nabla\vartheta(x)\,(< (\tau(x) - \mu(x))\nabla\vartheta(x), X(x) >).\end{aligned}$$

Finally, using the already proved condition (22) we have

$$\begin{aligned}\frac{d}{dt}\nabla\vartheta(x) &= (-DX(x)^T + \tau(x) - \mu(x))\nabla\vartheta(x) - \nabla\vartheta(x)\,(\tau(x) - \mu(x)) \\ &= -DX(x)^T\nabla\vartheta(x),\end{aligned}$$

as we wanted to prove. □

Remark 5.2. *It is clear that the classical Adjoint method considers $p \in \gamma$, then $\phi_t(p) = \gamma(t/T)$ with $\gamma(0) = p$.*

Remark 5.3. *We will see in the section devoted to the numerical implementation, that we will obtain a local approximation of the PRS semi-analytically by computing the parameterization K and using formula* (20)*. In order to obtain a PRS in a bigger domain, we will globalize the local approximation just integrating the adjoint problem equation* (21) *backwards.*

6. Solving the invariance equation

In [CFL05], the authors provide a method to solve the invariance equation (7) and they prove its convergence. In this section, we review the basic steps of the method and we refer the reader to [CFL05] for more details and the proof of the theorems.

In order to solve the invariance equation (7), we will discretize it in Fourier-Taylor series. Hence, we will first look for a K as a power series

$$K(\theta, \sigma) = \sum_{n=0}^{\infty} K_n(\theta)\sigma^n, \tag{25}$$

where the components of K_n are periodic functions of period 1, and then match the coefficients in σ^n on both sides of equation (7).

For $n = 0$, one obtains

$$\frac{1}{T}\frac{d}{d\theta}K_0(\theta) = X(K_0(\theta)) \tag{26}$$

which admits the solution $K_0(\theta) = \gamma(\theta)$, where γ is a parameterization of the limit cycle given in (2).

Remark 6.1. *Notice that if $K_0(\theta)$ is a solution, then $K_0(\theta + \omega)$ is also a solution for any $\omega \in [0, 1)$. Therefore, there is some ambiguity in parameterizing the phase of an oscillation, that can be avoided fixing the initial point corresponding to the zero phase. It can be fixed anywhere on the limit cycle. In the context of tonic spiking in neuroscience, for instance, it is common to fix $\theta = 0$ at the peak of the spike.*

For $n = 1$, we obtain

$$\frac{1}{T}\frac{d}{d\theta}K_1(\theta) + \frac{\lambda}{T}K_1(\theta) = DX \circ K_0(\theta)K_1(\theta), \tag{27}$$

which tells us that $K_1(\theta)$ is an eigenfunction with eigenvalue $-\lambda$ of the operator $\mathcal{L}$ defined by

$$\mathcal{L} := \frac{d}{d\theta} - TDX \circ K_0(\theta).$$

Using Proposition 5.2 in [CFL05], we know that $K_1(\theta)$ is a solution of the equation (27) with eigenvalue $-\lambda$ if and only if $K_1(0)$ is an eigenvector of the monodromy matrix Φ_1 with eigenvalue e^{λ}. The monodromy matrix can be computed by solving the first variational equation

$$\frac{d}{d\theta}\Phi_\theta = DX \circ K_0\Phi_\theta,$$

with $\Phi_0 = \mathrm{Id}$ and taking the value Φ_1.

Recall that for planar vector fields, the other eigenvector is given by the vector field $X(K_0(0)) = X(K_0(1))$ with associated eigenvalue 1.

Finally, it is easy to see that $K_1(\theta) = e^{\lambda\theta/T}\Phi_\theta K_1(0)$ is a solution of equation (27).

Remark 6.2. *For the numerical computations when the eigenvalue e^{λ} is very small, we will use that $\lambda = \int_0^T \mathrm{div}(X(\gamma(t/T)))dt$.*

Remark 6.3. *Notice that if $K_1(\theta)$ is a solution of equation (27), then $bK_1(\theta)$, for any $b \in \mathbb{R}$, is also a solution. Even though all the choices of $K_1(\theta)$ are mathematically equivalent, the choice affects the numerical properties of the algorithm. See Remark 7.2 for a more detailed discussion.*

For $n \geq 2$, we have

$$\frac{1}{T}\frac{d}{d\theta}K_n + \frac{n\lambda}{T}K_n = (DX \circ K_0)K_n + R_n \tag{28}$$

where R_n is an explicit polynomial in $K_0, \ldots, K_{n-1}$ whose coefficients are derivatives of X evaluated at K_0. These coefficients will be computed using the methods of automatic differentiation (see for instance [Gri00] and [JZ05]).

By Proposition 5.2 in [CFL05] the equation (28) for $n \geq 2$ can be solved provided that $e^{n\lambda}$ is not an eigenvalue of the monodromy matrix Φ_1 associated to γ. Notice that this assumption is satisfied for planar vector fields, provided that the limit cycle is hyperbolic, that is $\lambda \neq 0$.

Once $K_0(\theta)$ and $K_1(\theta)$ are fixed (see Remarks 6.1 and 6.3), the solution $K_n(\theta)$ for $n \geq 2$ of equation (28) is uniquely determined. Taking into account that K_n are periodic solutions in θ, we will discretize the equation (28) using Fourier series and reduce the problem to solve a linear system in the Fourier space, see Section 7 for more details.

Finally, by Theorem 5.4 in [CFL05] we know that, provided that λ satisfies the mentioned conditions, the series constructed here converges to a true analytic solution of the problem.

7. Numerical implementation of the method

In the previous sections we have described the method, but there are many numerical details which are important and nontrivial. They do not depend on the method but they are inherent to the problem. In this section we provide some details about the implementation we have carried out.

7.1. **Fourier-Taylor discretization.** In order to solve equation (7), we will discretize the invariance equation using **Fourier-Taylor series** and study numerical methods to solve the discretized equations.

As we already mentioned in Section 6, we first seek K as a power series

$$K(\theta, \sigma) = \sum_{n=0}^{\infty} K_n(\theta)\sigma^n,$$

where $K_n(\theta)$ are 1-periodic functions in θ. Thus, using Fourier formalism, the $K_n(\theta)$ can be written as

$$K_n(\theta) = \sum_{k\in\mathbb{Z}} c_k^n e^{2\pi i k\theta}.$$

Since we deal only with real functions, we only need to store half of the coefficients or, equivalently, store the cosine and sine Fourier series:

$$K_n(\theta) = a_0^n + \sum_{k>0} a_k^n \cos(2\pi k\theta) + b_k^n \sin(2\pi k\theta),$$

where $a_0 = c_0^{re}$, $a_k = 2c_k^{re}$ and $b_k = -2c_k^{im}$ for $k > 0$.

In the numerical implementation we need to truncate these expansions. In order to decide up to which order N we compute the Fourier series we require that the residuals are of size of order $10^{-15} - 10^{-20}$. That is, we truncate the Fourier series up to some order N in such a way that the norm of the last 10 per cent of Fourier coefficients is smaller that the considered order, in symbols

$$|K_n^{tail}| = \sum_{k=\lfloor 0.9N/2 \rfloor}^{N/2} |a_k^n| + |b_k^n| < 1.0e-15. \tag{29}$$

Remark 7.1. *One of our goals is to apply this method to classical systems in neuroscience. The main practical shortcoming in these cases is that the Fourier series are not adaptable to the usual presence of spikes (slow-fast systems), where the Fourier coefficients decrease very slowly and not uniformly. Although these systems can be analytic, from this numerical point of view they behave as if they were not. In these cases, other methods of discretization which are more adaptive like splines or wavelets could give some improvements.*

Since the vector field is assumed to be analytic, so it can be written using algebraic operations and elementary transcendental functions, we can use automatic

differentiation algorithms (see [Gri00], [JZ05]) to obtain Taylor expansions of the operators in (7).

In the whole process when we have a discretization of a periodic function in the real space, we use the Fast Fourier Transform (FFT) to compute the Fourier series. In this work we have used the `fftw3` library (see http://www.fftw.org/).

7.2. **Discretization of the invariance equation and accuracy of the solution.** We will solve the invariance equation (7) by solving equations (26), (27) and (28) for $n \geq 2$. Observe that equations (26) and (27) are special because they involve four unknowns $(K_0(\theta), T, K_1(\theta), \lambda)$. These two equations will be solved simultaneously using additional information. Instead, equation (28) can be treated the same way for any $n \geq 2$.

In order to solve equations (26) and (27) we will need to integrate the system of ODEs. The integration method used is a Taylor method (we have used the routines provided by Jorba and Zou, see [JZ05] and

http://www.maia.ub.es/~angel/soft.html).

We used adaptive step size and degree and a tolerance (absolute and relative) of 1.0e-16.

Recall that for $n = 0$ we need to look for a periodic solution. In order to compute it, we consider a Poincaré section and reduce the problem to find a zero of the Poincaré map that can be achieved using a Newton method. Note that for the Newton method we will need to integrate the variational equations together with the vector field. The solution for the variational equations will be used to solve equation (27) according to the method explained in Section 6.

Once we obtain the limit cycle $K_0(\theta)$ and $K_1(\theta)$ we store them for equidistant values of θ, that is $\theta_i = i/N$, for $i = 0, \ldots, N-1$.

For $n \geq 2$ the most straightforward method is to discretize (28) using a basis of N Fourier coefficients and, then, apply a linear solver. However, once we have obtained K_0 and K_1, we can perform a change of coordinates given by $(x, y) = g(\theta, \sigma) = K_0(\theta) + \sigma K_1(\theta)$. If we apply the method again to the system obtained after this change, then it turns out that the equation (28) becomes diagonal in Fourier series. Once we obtain the solution as a Fourier series we can go back to real space using the Fast Fourier Transform. Again, as in the previous cases we store K_n for equidistant values of θ.

An alternative method consists of applying a quasi-Newton method to the invariance equation.

By now, the results shown in Section 9 have been obtained using the straightforward method.

To check the accuracy of the solutions K_n obtained, we substitute them in the corresponding equation ((26) if $n = 0$, (27) if $n = 1$ and (28) if $n \geq 2$) for discrete values of $\theta_i = i/N$, for $i = 0, \ldots, N-1$. For each value of θ, this substitution provides an evaluation of the error $E_n(\theta)$. Finally, we evaluate the discrete ℓ_1 norm of $\{E_n(\theta_i)\}_{i=0}^{N-1}$ to get the accuracy; that is

$$\|E_n\| = \frac{1}{N} \sum_{i=0}^{N-1} |E_n(\theta_i)|. \tag{30}$$

Notice that the computation of $E_n(\theta_i)$ involves again a FFT.

7.3. **Local approximation of the isochrons.** Once we have solved the invariance equation up to order L we have obtained a local approximation of the stable invariant manifold. It remains to determine the domain of convergence and the order of the error of the local approximation. Both concepts are very strongly related.

Given an approximate solution

$$K^{[\leq L]}(\theta,\sigma)=\sum_{n=0}^{L}K_n(\theta)\sigma^n, \tag{31}$$

where

$$K_n(\theta)=a_0^n+\sum_{k=1}^{N/2}a_k^n\cos(2\pi k\theta)+b_k^n\sin(2\pi k\theta),$$

The radius of convergence $r=1/l$ for the Taylor series is given by

$$l=\lim_{n\to\infty}\frac{\|K_{n+1}\|}{\|K_n\|},$$

where $\|\cdot\|$ denotes the ℓ_1 norm defined in (30). Thus, a direct strategy to compute l could be imposing that $|l_n-l_{n-1}|<\epsilon$, for some prescribed $\epsilon>0$, where $l_n=\|K_{n+1}\|/\|K_n\|$. Then, $r=1/l_n$ could be a numerical approximation of the theoretical radius of convergence. However, for numerical reasons, the radius can shrink in practical implementation. Consequently, we compute the convergence region in an alternative way.

For each θ we compute a value $\sigma_0(\theta)$ such that the approximate solution $K^{[\leq L]}(\theta,\sigma)$ given in (31) solves the invariance equation (7) up to a certain error E, that we established between $10^{-10}-10^{-12}$. That is, we fix θ and we compute the values of $\sigma\in\mathbb{R}$ such that

$$\left|\frac{1}{T}\sum_{n=0}^{L}K_n'(\theta)\sigma^n+\frac{\lambda}{T}\sum_{n=0}^{L}nK_n(\theta)\sigma^n-X\left(\sum_{n=0}^{L}K_n(\theta)\sigma^n\right)\right|<E, \tag{32}$$

where

$$K_n'(\theta)=2\pi\sum_{k=1}^{N/2}kb_k^n\cos(2\pi k\theta)-ka_k^n\sin(2\pi k\theta).$$

Remark 7.2. *Recall that if $K(\theta,\sigma)$ is a solution of the invariance equation (7) so is $K(\theta+\omega,b\sigma)$, for any $\omega\in[0,1)$ and $b\in\mathbb{R}$. As we already mentioned in Remark 6.1 the choice of ω is related to the zero phase for the limit cycle. So, following the usual criterion in neuroscience, we will fix the zero phase for the oscillator at the spike. The choice of b is related to the domain of convergence. Hence, if we choose a large b the domain where we can evaluate the series will be small. Although mathematically we can choose any value of b, for the numerical stability it will be convenient to choose a value of b such that the coefficients K_n can be kept at order 1, so that one can avoid the round-off errors. Notice that if we consider bK_1 then new K_n is b^nK_n.*

However, in some cases, the K_n do not converge uniformly and in these cases one can not find a global b. The immediate consequence of this fact is that for some values of θ, the K_n become smaller than the machine precision and one can not trust them. For these values, increasing the order L of the Taylor polynomial has no effect on increasing the domain where the local approximation is reliable.

7.4. **Globalizing the manifold.** In theory, the method presented here gives a parameterization of the whole manifold. However, we have seen that, numerically, given an error bound $(10^{-10} - 10^{-12})$, we can compute the isochron only up to a value $\sigma = \sigma_0(\theta)$ for each θ.

A standard way to extend local approximations obtained semi-analytically is to globalize them using the dynamics given by the vector field (see [Sim90]).

Typically, given a point $\gamma(\theta_0)$ on the limit cycle, one could take n points parameterized by (θ_0, σ) with $\sigma \in (\sigma_0(\theta_0)e^{\lambda}, \sigma_0(\theta_0))$, on the corresponding isochron and then perform iterates of the inverse time-T map Φ_{-T} for these points, where here Φ_t denotes the flow of X. However, in many cases (included models in neuroscience in which we are specially interested) this method has the disadvantage that we get too many points close to $\gamma(\theta_0)$ and just a few far from it. Moreover, some of them may escape very fast far from the limit cycle.

This last shortcoming can be avoided using that isochrons, even if they are not invariant, they are preserved by the flow, that is isochrons are carried into isochrons. Hence, we can consider inverse time-$T\Delta\theta$ maps $\Phi_{-T\Delta\theta}$ as well as, taking $\Delta\theta = 1/n$, $n \in \mathbb{N}$, n local invariant manifolds corresponding to $\gamma(\theta_0 + j\Delta\theta)$, for $j = 0, \ldots, n-1$. Then, to globalize the isochron corresponding to $\gamma(\theta_0)$ we obtain points $\{p_0, \ldots, p_m\}$ on it from points on the local approximation of other isochrons parameterized by $(\theta_0 + k_m\Delta\theta, \sigma_m)$, such that

$$p_m = \Phi_{-k_m T\Delta\theta}(K(\theta_0 + k_m\Delta\theta, \sigma_m)) \tag{33}$$

with $k_m \in \mathbb{N}$.

The method to decide which σ_m and k_m we choose to compute each p_m in order to get points on the globalized isochron less sparse, is based on a method given in [Sim90] (see also [KO98] for another alternative). For the sake of completeness, we explain the details of the method adapted to our purpose.

We want to extend the local isochron for a phase θ_0. We are going to approximate it by a sequence of points $\{p_0, \ldots, p_m\}$ on the isochron for which we will assume that they are at a distance smaller than some tolerance Δs, that is

$$\|p_m - p_{m-1}\| < \Delta s,$$

and the angle between three consecutive points is bigger than a certain tolerance $\Delta\alpha$,

$$(p_{m-1} - p_{m-2}) \cdot (p_m - p_{m-1}) \geq \cos(\Delta\alpha)\|p_{m-1} - p_{m-2}\|\|p_m - p_{m-1}\|.$$

Assume that we have computed up to p_m satisfying the previous conditions and we have a current value of σ_m and $\Delta\sigma_m$ such that $\sigma_m = \sigma_{m-1} + \Delta\sigma_m$ and a certain iterate k such that

$$\Phi_{-kT\Delta\theta}(K(\theta_0 + k\Delta\theta, \sigma_m)) = p_m.$$

We want to predict the new σ_{m+1} and therefore $\Delta\sigma_{m+1}$, such that

$$\Phi_{-kT\Delta\theta}(K(\theta_0 + k\Delta\theta, \sigma_m + \Delta\sigma_{m+1})) = p_{m+1},$$

satisfying that it is at a distance smaller than Δs from p_m.

Then, we consider

$$\Delta\sigma_{m+1} = \min\left(\frac{\Delta s}{\Delta s_m}, \frac{\Delta\alpha}{\Delta\alpha_m}, 1.5\right)\Delta\sigma_m\, 0.8$$

where Δs_m is the distance between p_{m-1} and p_m and $\Delta\alpha_m$ the angle between $\bar{v} = p_{m-1} - p_{m-2}$ and $\bar{w} = p_m - p_{m-1}$. The factor 0.8 can be seen as a security factor.

If $\sigma_{m+1} = \sigma_m + \Delta\sigma_{m+1}$ falls into the allowed range for σ, that is $\sigma_{m+1} < \sigma_0(\theta_k)$, where $\theta_k = \theta_0 + k\Delta\theta$, which means that we are in the range where the local approximation of the isochron for θ_k is good, we integrate for $\Phi_{-kT\Delta\theta}$ and we obtain p_{m+1}. In this case we define $k_{m+1} = k$ according to (33).

Otherwise, we keep dividing both σ_{m+1} and $\Delta\sigma_{m+1}$ by $e^{\lambda\Delta\theta}$ l times until $\sigma_{m+1} \leq \sigma_0(\theta_{k+l})$. We say then that $k_{m+1} = k+l$ and we compute p_{m+1} from (33). Typically, $l = 1$ but it can be greater. We replace k by $k + 1$.

If despite our choice of $\Delta\sigma_m$ the point p_{m+1} obtained fails to satisfy one of the conditions, we can either consider a smaller $\Delta\sigma_{m+1}$ (taking into account that the $\Delta\sigma$'s cannot be smaller than a certain value $\Delta_{\min}$) or keep the computed point and use an interpolation method for this part.

Remark 7.3. *We can globalize the PRS in parallel with the isochrons: we approximate them locally according to* (20) *and we globalize them integrating the system* (21) *backwards together with the vector field.*

7.5. **Software.** The algorithms have been implemented in C language and have been run under the Linux environment. They have been applied to compute isochronous sections and PRCs of limit cycles for planar vector fields which appear in models of neuroscience and neurobiology.

The program performs the following steps: (1) Computation of the limit cycle and its period, the monodromy matrix and the characteristic exponent. (2) Computation of the Fourier-Taylor expansions of the isochrons (3) Computation of the domain of convergence and the local approximation for the isochrons and the PRS (4) Globalization of the isochrons and the PRS. The figures are obtained using `gnuplot` and `Matlab`.

8. Isochronous sections, (un)stable manifolds and foliations in $\mathbb{R}^n$

Although computing isochronous sections of limit cycles in $\mathbb{R}^n$, for $n \geq 3$, is beyond the scope of this paper, we would like to highlight the main differences with the planar case. The effective computation in higher dimensions is a goal for future work.

The theoretical extension to higher dimensions can be derived in a straightforward manner, though the practical implementation encompasses a plethora of new challenges. Here, we give the theoretical ideas and concepts, together with comments concerning practical issues.

Definition 8.1. *Let us consider a smooth system of differential equations*

$$\dot{x} = X(x), \qquad x \in \Omega, \quad \Omega \in \mathbb{R}^n, \quad n \geq 2,$$

with a hyperbolic limit cycle $\gamma : \mathbb{R} \mapsto \mathbb{R}^n$. An isochronous section *of γ is a hypersurface Σ of $\mathbb{R}^n$ (dimension $n-1$) such that*

$$x \in \Sigma \Leftrightarrow \varphi_T(x) \in \Sigma$$

where $\varphi_t(x)$ is a solution of X such that $\varphi_0(x) = x$, and T is the period of the limit cycle γ.

To extend the theoretical results, it is convenient to refer to *integrable systems* (see [Olv93]):

Definition 8.2. *Let $Y_1, \ldots, Y_r$ be vector fields on a smooth manifold M. An* integral submanifold *of $\{Y_1, \ldots, Y_r\}$ is a submanifold $N \subset M$ whose tangent space $TN|_x$ is spanned by the vectors $\{Y_1|_x, \ldots, Y_r|_x\}$ for each $x \in N$. The system of vector fields $\{Y_1, \ldots, Y_r\}$ is* integrable *if through every point $x_0 \in M$ is contained in an integral submanifold.*

Thus, having a neighborhood $\Omega \subset \mathbb{R}^n$ of γ filled by isochrons is equivalent to having an integrable system of vector fields $\{Y_1, \dots, Y_r\}$, with $r = n-1$ defined in this neighborhood. One way to obtain these vector fields Y_j is to impose (see [FGG07]) that $[Y_j, X] = \mu_j Y_j$, for $j = 1, \dots, n-1$. However, as Frobenius theorem shows, this requirement is not sufficient: the $n-1$ vector fields have to be in involution.

We recall both the definition of involution and Frobenius theorem (see also [Olv93]):

Definition 8.3. *A system of vector fields $\{Y_1, \dots, Y_r\}$ on M is* in involution *if there exist smooth real-valued functions $h_{ij}^k(x)$, $x \in M$, $i,j,k = 1, \cdots, r$, such that for each $i, j = 1, \cdots, r$,*

$$[Y_i, Y_j] = \sum_{k=1}^{r} h_{ij}^k \cdot Y_k.$$

Theorem 8.4 (Frobenius)**.** *Let $Y_1, \dots, Y_r$ be smooth vector fields on M. Then, the system $\{Y_1, \dots, Y_r\}$ is integrable if and only if it is in involution.*

Summing up, adapting Frobenius theorem to our problem, we have:

Theorem 8.5. *Let us consider a smooth system of differential equations*

$$\dot{x} = X(x), \qquad x \in \Omega, \qquad \Omega \in \mathbb{R}^n, \qquad n \geq 2,$$

with a hyperbolic limit cycle $\gamma\colon \mathbb{R} \mapsto \mathbb{R}^n$. Suppose that there exist $n-1$ non-trivial vector fields $Y_1, \dots, Y_{n-1}$ in involution such that

$$[Y_j, X] = \mu_j Y_j \qquad j = 1, \dots, n-1$$

for scalar functions $\mu_j\colon \mathbb{R} \mapsto \mathbb{R}^n$, $j = 1, \dots, n-1$. Then, the isochronous sections are the maximal integral submanifolds of the integrable system of vector fields $\{Y_1, \dots, Y_{n-1}\}$.

The integral submanifolds themselves are referred to as *leaves* of the *foliation* of Ω.

When $n > 2$, it may happen that a limit cycle has both stable and unstable manifolds. Let $n_s = \dim W_s(\gamma)$ and $n_u = \dim W_u(\gamma)$. Using the parameterization method or other computational techniques, we can obtain both $W_s(\gamma)$ and $W_u(\gamma)$ numerically. In other words, we would be computing the leaves of the partial foliations given by the systems $\{Y_1, \dots, Y_{n_s}\}$ (resp., $\{Y_{n_s+1}, \dots, Y_{n_s+n_u}\}$), where $\int_\gamma \mu_j < 0$ (*resp.*, > 0) if $j = 1, \dots, n_s$ (resp., $j = n_s+1, \dots, n_s+n_u$). However, this does not give the whole foliation of the neighborhood.

A more suitable formulation to characterize the isochronous leaves can be obtained by using differential geometry notation. For the sake of simplicity, we only give a sketch of it and we restrict ourselves to $\mathbb{R}^2$ though it can be extended to $\mathbb{R}^n$.

Consider a vector field $X := P(x,y)\frac{\partial}{\partial x} + Q(x,y)\frac{\partial}{\partial y}$ and its associated 1-form $\omega_X := -Q(x,y)\,dx + P(x,y)\,dy$. We recall that $i_X\,\alpha$ denotes the contraction (interior product) of a k-form α with respect to X which gives a $(k-1)$-form. In particular, any vector field and its associated 1-form are related by $i_X\,dx \wedge dy = \omega_X$.

It is known from classical tensor calculus (see formula 1.62 in [Olv93]) that

$$i_{[X,Y]}\,\omega = X(i_Y\,\omega) - i_Y(X(\omega)), \tag{34}$$

for any k-form ω. If we use that $[Y, X] = \mu\, Y$ and choose $\omega = \omega_Y$, the left-hand side of (34) becomes

$$i_{[Y,X]}(\omega_Y) = i_{\mu\, Y}(\omega_Y) = \mu\, i_Y(\omega_Y).$$

Using now that $i_Y(\omega_Y) = 0$, we can write (34) as $i_Y(X(\omega_Y)) = 0$ or, equivalently,

$$X(\omega_Y) = \lambda(x, y)\,\omega_Y, \tag{35}$$

for some function λ. Thus, the problem of finding isochrons is equivalent to finding a 1-form ω_Y and a function λ satisfying (35). The leaves of ω_Y will then be the isochronous sections of the limit cycle.

9. Examples

In this section, we apply our method to representative examples, ranging from the most simple instances of Hopf and SNIC (saddle-node on an invariant curve) bifurcations and the classical van der Pol oscillator to more sophisticated neuronal models. Apart from obtaining isochrons, PRCs and PRSs, through these examples we want to illustrate different facts: (a) what are the clues to explain the transition from "Type 1" PRCs to "Type 2" PRCs; (b) the numerical problems that arise when dealing with slow-fast systems; and, (c) up to which degree PRSs show disagreement with PRCs in the same phase and how this can affect high frequency stimulation. We end the paper with a discussion on these facts in Section 10.

We start with a direct application to the simplest vector fields that exhibit either a Hopf or a SNIC bifurcation, for which we can compute their limit cycle and the corresponding normalizing vector field analytically and we can also get an analytic expression for the PRC.

Example 9.1. *We consider a simple example of a supercritical Hopf bifurcation*

$$\begin{cases} \dot{x} &= \beta x - y - x(x^2+y^2), \\ \dot{y} &= x + \beta y - y(x^2+y^2), \end{cases} \tag{36}$$

which writes, in polar coordinates, as

$$\begin{cases} \dot{r} &= r(\beta - r^2), \\ \dot{\theta} &= 1. \end{cases}$$

For $\beta = 0$, there is a supercritical Hopf bifurcation giving rise, for $\beta > 0$, to a stable limit cycle γ of radius $\sqrt{\beta}$ and period 1. We parameterize γ by θ in the following way:

$$\gamma(\theta) = (\sqrt{\beta}\cos(\theta), \sqrt{\beta}\sin(\theta)).$$

It is not difficult to see that the vector field $Y(x, y) = (x, y)$ and the function $\mu(x, y) = -2(x^2 + y^2)$ satisfy the condition (4).

Hence, taking into account that $Y^\perp = (-y, x)$ and $< Y^\perp, X >= x^2 + y^2$, by equation (18) *the phase shift for a point $p = (x, y) \in \Omega$ is given by*

$$\nabla\vartheta(p) = \left(-\frac{y}{x^2+y^2}, \frac{x}{x^2+y^2}\right).$$

Then, using the parameterization of the limit cycle, the PRC is just

$$\nabla\vartheta(\gamma(\theta)) = \frac{1}{\beta}(-\sqrt{\beta}\sin(\theta), \sqrt{\beta}\cos(\theta)).$$

That is, $PRC_1(\theta) = -\sin(\theta)/\sqrt{\beta}$, and $PRC_2(\theta) = \cos(\theta)/\sqrt{\beta}$.

Example 9.2. *The easiest way to obtain a saddle node on an invariant cycle bifurcation bifurcation is through*

$$\begin{cases} \dot{r} &= r(\beta - r^2), \\ \dot{\phi} &= m - \sin(\phi), \end{cases} \tag{37}$$

which, in cartesian coordinates, writes as

$$\begin{cases} \dot{x} &= \beta x - my - x(x^2+y^2) + \frac{y^2}{\sqrt{x^2+y^2}}, \\ \dot{y} &= m\,x + \beta y - y(x^2+y^2) - \frac{xy}{\sqrt{x^2+y^2}}. \end{cases}$$

We assume that $\beta > 0$ and $m > 1$. Therefore, there exists a unique and stable circular limit cycle γ of radius $\sqrt{\beta}$ that we parameterize by a phase θ satisfying $\dot{\theta} = 1/T$, $\theta \in [0,1)$ in the following way

$$\gamma(\theta) = (\sqrt{\beta}\cos(\Omega(\theta)), \sqrt{\beta}\sin(\Omega(\theta))),$$

where Ω is the phase transformation between θ and ϕ, given by the solution of the Cauchy problem

$$\frac{1}{T}\frac{d\Omega}{d\theta} = m - \sin(\Omega(\theta)); \quad \Omega(0) = 0.$$

The explicit solution can be obtained analytically,

$$\Omega(\theta) = 2\arctan\left(\frac{m\sin(\frac{T}{2}\sqrt{m^2-1}\,\theta)}{\sqrt{m^2-1}\cos(\frac{T}{2}\sqrt{m^2-1}\,\theta) + \sin(\frac{T}{2}\sqrt{m^2-1}\,\theta)}\right). \tag{38}$$

Again, as in Example 9.1, the vector field $Y(x,y) = (x,y)$ and the function $\mu(x,y) = -2(x^2+y^2)$ satisfy condition (4).

Hence, taking into account that $Y^\perp = (-y,x)$ and

$$< Y^\perp, X >= m(x^2+y^2) - y\sqrt{x^2+y^2},$$

by equation (18) PRCs are given by

$$\nabla\vartheta(\gamma(\theta)) = \frac{1}{\beta(m-\sin(\Omega(\theta)))}(-\sqrt{\beta}\sin(\Omega(\theta)), \sqrt{\beta}\cos(\Omega(\theta))).$$

That is,

$$PRC_1(\theta) = -\frac{\sin(\Omega(\theta))}{\sqrt{\beta}\,(m-\sin(\Omega(\theta))},$$

see Fig. 1, and $PRC_2(\theta) = \frac{\cos(\Omega(\theta))}{\sqrt{\beta}\,(m-\sin(\Omega(\theta))}$.

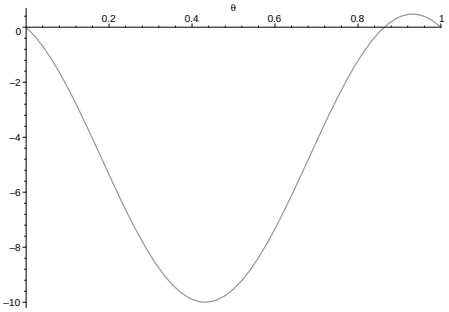

FIGURE 1. PRC_1 for system (37) with $m = 1.1$, $\beta = 1$. Phase has been scaled to $[0,1]$. Observe the slightly positive bump when $\theta \in (0.9, 1)$ approx.

9.1. **Numerical examples.** We present here an application of our models to a set of examples we found relevant either to illustrate the properties or because they are representative of classical models:

1. The Van der Pol oscillator:

$$\begin{cases} \dot{x} &= -y + x - x^3, \\ \dot{y} &= x. \end{cases} \tag{39}$$

2. A reduced Hodgkin-Huxley-like system, with sodium and potassium currents, and only one gating variable:

$$\left\{\begin{array}{ll}\dot{V} & =\frac{-1}{C_m}(g_{Na}m_\infty(V)(V-V_{Na})+g_K n(V-V_K)+g_L(V-V_L)-I_{app}),\\ \dot{n} & =n_\infty(V)-n,\end{array}\right. \tag{40}$$

where V represents the membrane potential, n is a gating variable, the open-state probability functions are

$$m_\infty(V)=\frac{1}{1+\exp(-(V-V_{max,m})/k_m)}\,,$$

$$n_\infty(V)=\frac{1}{1+\exp(-(V-V_{max,n})/k_n)}\,,$$

and the parameters are $C_m=1.$, $g_{Na}=20.$, $V_{Na}=60.$, $g_K=10.$, $V_K=-90.$, $g_L=8.$, $v_L=-80.$, $V_{max,m}=-20.$, $k_m=15.$, $V_{max,n}=-25.$, $k_n=5$.

3. The Selkov model (see [Sel68]), initially a model for self-oscillations in glycolysis, which has also been extensively used in models for circadian rhythms (see for instance [DN94] and [PZG07]). It is given by

$$\left\{\begin{array}{ll}\dot{x} & =1-x\,y,\\ \dot{y} & =a\,y\,(x-(1+b)/(1+b\,y)),\end{array}\right. \tag{41}$$

where the parameters are $a, b\in\mathbb{R}$.

4. The Morris-Lecar model (see [ML81]), initially conceived as a model for a barnacle giant muscle fiber, but well-studied in the neuroscience literature (after [RE98]) as a paradigm for the different bifurcations that give rise to limit cycles. The model is given by:

$$\left\{\begin{array}{ll}\dot{V} & =\frac{1}{C}\left(I-g_L(V-V_L)-g_K\omega(V-V_K)-g_{Ca}m_\infty(V)(V-V_{Ca})\right),\\ \dot{w} & =\phi\frac{w_\infty(V)-w}{\tau_w(V)},\end{array}\right. \tag{42}$$

where

$$m_\infty(V)=\frac{1}{2}(1+\tanh((V-V_1)/V_2)),$$

$$w_\infty(V)=\frac{1}{2}(1+\tanh((V-V_3)/V_4)),\text{ and}$$

$$\tau_w(V)=(\cosh((V-V_3)/(2V_4)))^{-1}\,,$$

and the parameters are $V_L=-60$, $V_K=-84$, $V_{Ca}=120$, $V_1=-1.2$, $V_2=18$, $V_3=2$, $V_4=30$, $g_L=2$, $g_K=8.0$, $g_{Ca}=4.4$, $C=20$ and $\phi=0.04$.

All these examples share common characteristics with slight differences that will be remarked at the end of this section. Let us start, then, with the common features.

9.1.1. *Common features: methods, parameter values and figure labelling.* In all the cases, we are interested in studying the dynamics close to a hyperbolic limit γ of period T that surrounds an unstable critical point p^*. The zero phase point on γ is the point which has a maximum value of the first component (x or V depending on the example). As in previous sections, we call λ the characteristic exponent of γ (so, the characteristic multiplier is e^λ). The computation of the periodic orbits has been performed using a Newton method with a tolerance of $1.0e-15$. In the neighborhood of γ, we have performed a Taylor expansion as in (31) up to order L and we have considered N Fourier modes for the K_n. With them we obtain residuals for the K_n as defined in (29), which are of order $|K_n|_{tail}$. The local approximation

that we get for the isochrons defined in (32) is computed with an error smaller than E_{loc}, while the globalization of the manifold has been performed following (33) and using a Taylor method with a tolerance of order $1.0e-16$. In the globalization (see definitions after (33)), we require a distance of order $\Delta s = 1.0e-2$ between two consecutive points on the isochron and we fix $\Delta_{min} = 1.0e-8$ and $\Delta\alpha = 0.3$.

Values for each example of all the parameters defined in the last paragraph are given in Table 1. All the results will be given with 4 significant digits although all the computations have been performed with double precision.

Model	Figure	$T \approx$	$\lambda \approx$	$L =$	$N =$	$E_{tail} \in$	$E_{loc} =$
1	2	6.663	-7.059	15	2^8	$(10^{-20}, 10^{-15})$	10^{-12}
2, I=10	3	7.074	-27.66	5	2^{11}	$(10^{-17}, 10^{-12})$	10^{-8}
2, I=165	4	1.630	-3.384	10	2^9	$(10^{-19}, 10^{-14})$	10^{-10}
3	5	6.344	-4.909	15	2^9	$(10^{-16}, 10^{-14})$	10^{-11}
4	6	99.27	-9.122	5	2^{10}	$(10^{-20}, 10^{-13})$	10^{-8}

TABLE 1. Parameter values for the different models: T=period of the orbit γ; λ=characteristic exponent associated to γ; L=order of the Taylor expansion; N=number of Fourier modes; $|K_n^{tail}|$=residuals for the K_n; E_{loc}=maximum error when computing local approximation of isochrons.

For each model, we present a figure (Figs. 2 to 6) with different panels. In order to compact notation, we label each panel with a different symbol: (`Kn`), (`Iso`), (`PRC`), (`PRS`) and (`PR`θ).

In panels (`K`), the computed K_n, for some values of n, are shown. The fact that the orbits do not approach γ uniformly in θ has the effect that for certain values of θ, as n goes to infinity, the value of K_n goes to zero faster than for other values, see the slow-fast item in Section 10 for a discussion on this question.

In panels (`Iso`) we plot the isochrons corresponding to the phases j/N_ϕ, for $j = 0, \ldots, N_\phi - 1$, with $N_\phi = 16$, typically. We show the local approximation (green) computed semi-analytically using the parameterization method and the globalized isochron (red) using the dynamics given by the vector field. We restrict the computation to a rectangular domain $\mathcal{R}$ containing the limit cycle.

In panels (`PRC`) we plot the PRC_1 (green) and the PRC_2 (blue) for an infinitesimally small perturbation in the directions $(1, 0)$ and $(0, 1)$, respectively, with a certain amplitude specified in each figure caption, jointly with the x (or V) component (red line) of the oscillator (scaled for a better reference). Notice that the PRC_1, corresponding to the horizontal pulses, is just the section with $\sigma = 0$ of PRSs that are given in panels (`PRC`).

In panels (`PRS`), we plot the PRS_1 in the variables θ and σ, but only for positive values of σ, avoiding negative values for the sake of clearness. The positive values of σ correspond to the points (x, y) in the external part of the limit cycle (depending on the orientation of the limit cycle, the sign of σ defined by the parameterization method out of the limit cycle can be also negative; in these figures we change $\sigma \mapsto -\sigma$ for the sake of homogeneity). Indeed, in these panels we plot the phase shift for the points (x, y) in the outer neighborhood of the limit cycle displayed in panels (`Iso`). Since we restrict to the rectangular domain $\mathcal{R}$ in the variables (x, y) (because they are the "real" phase space variables), when plotting the PRS in the variables (θ, σ), we come across with a non-regular domain. On the top of

that, sometimes the discretization of local isochrons (Δs) used to globalize other isochrons undergoes the limit Δ_{min} and cannot longer extend the isochron. This is why some isochrons do not reach the border of the rectangular domain $\mathcal{R}$.

Like the isochrons, the PRS_1s are computed locally using semi-analytical methods and extended by integrating the system (21), see Section 7.4. Thus, the mesh is not completely regular, so we have used cubic interpolation with splines in order to show it in an regular grid on the plane (θ, σ).

Although the PRSs contain the maximum information about phase advancement, sometimes they are not easy to visualize. Accordingly, we have decided, in some cases, to show sections of the PRSs with fixed phases (that is, $\theta = \theta^*$ and parameterized by σ). Using this view, we can easily illustrate the differences in phase advancement between different points on the same isochron. These panels are labelled as ($\mathtt{PR}\theta$).

Before entering into the discussion, we go through the non-common features of each example.

Remark 9.3. *For the Hodgkin-Huxley-like model* (40)*, we have studied the system in two regimes:* $I_{app} = 10$ *(close to a SNIC bifurcation which occurs at* $I_{app} \approx 4.513$*) and* $I_{app} = 165$ *(closer to a Hopf bifurcation which occurs at* $I_{app} \approx 213.8$*). Bifurcation values are obtained through* XPPAUT*, see* [Erm02].

For the case $I_{app} = 10$*, which is the case close to SNIC, the system presents a slow-fast dynamics that will accentuate some of the problems that we already mentioned in the previous example. In this case, we computed the Taylor expansion up to order* $L = 5$*, because, as we can appreciate in Fig. 3, for some values of* θ*, as* n *increases the* K_n *tend to zero much faster. Moreover, since the functions* K_n *present very sharp spikes we need to consider up to* $2^{10} = 1024$ *or* $2^{11} = 2048$ *Fourier modes to get good approximations, that is with residuals smaller than a certain error. This implies solving linear systems with large matrices that are not very stable.*

Notice that this limit cycle is "strongly" hyperbolic and the backwards integration can be somehow very unstable.

The system presents a fixed point at $(-26.83, 0.4093)$*, which is computed using a Newton method with a tolerance of* $1.0e-13$*.*

Once can appreciate in Fig. 3 that the isochrons computed semi-analytically (green ones, hardly noticeable) are shorter than in the Hopf case (Fig. 4). In this case, in order to have a long enough local approximation for the isochrons we reduced the accuracy of the computation down to $1.0e-08$*.*

For the case $I_{app} = 165$*, which is close to the Hopf bifurcation, in Fig. 4 one can observe that the slow-fast phenomenon that we mentioned above is softened.*

The system presents a hyperbolic fixed point for at $(-21.00, 0.6899)$*, which has been computed numerically with an error smaller than* $1.0e-13$*.*

Remark 9.4. *The Selkov model* (41) *presents an Andronov-Hopf bifurcation for* $a = (1+b)/b$*. We have studied here the case* $a = 3$*,* $b = 1$*. The unstable fixed point, that can be easily computed analytically, is located at* $(1, 1)$*.*

In this example, we have decided to allow $\Delta_{max} = 1.0e-12$ *because far from the limit cycle points escape.*

Remark 9.5. *For the Morris-Lecar model* (42)*, we have considered the case* $I_{app} = 91$*, which presents similar issues as the 2D Hodgin-Huxley model close to a SNIC considered above.*

The system has a fixed point at $(-26.26, 0.1320)$*, which is computed using a Newton method with a tolerance of* $1.0e-13$*.*

It is to be noticed that equation (42) *presents a subcritical Hopf bifurcation at* $I_{app} \approx 93.86$*; the unstable limit cycle goes "back" in the parameter space up to* $I_{app} \approx 88.29$*, where it coalesces with a stable limit cycle in a bifurcation of a semistable limit cycle that disappears for lower* I_{app}*'s. The stable limit cycle, which comes from another bifurcation for some* $I_{app} \gg 93.86$*, is the one that we study. It can be checked that the period of this stable orbit is notably above of that of the unstable orbit, born at the subcritical Hopf bifurcation; thus, one may expect a more slow-fast dynamics, more similar to a limit cycle close to a SNIC bifurcation than to a Hopf bifurcation.*

Some of the shortcomings of the Hodgkin-Huxley close to a SNIC are reproduced also here: it is necessary to solve linear systems with large matrices that are not very stable; the limit cycle is "strongly" hyperbolic and the backwards integration can be somehow very unstable; to have a long enough local approximations for the isochrons we need to reduce the accuracy of the computation.

Another specific observation is that the isochrons spiral around the unstable limit cycle in the interior of the stable one. This is not surprising since the two limit cycles have different periods and so, they cannot share the system of isochrons. Next short example illustrates analytically this fact.

Example 9.6. *Consider the* $\mathcal{C}^1$ *system in polar coordinates*

$$X := \begin{cases} \dot{r} &= r\, a(r), \\ \dot{\theta} &= b(r). \end{cases}$$

Suppose that $a(r_j) = 0$*,* $a'(r_j) \neq 0$ *and* $b(r_j) \neq 0$*, for* $j = 1, 2$*, with* $r_1 \neq r_2$*, both positive.*

It is straightforward to see that $\{r = r_1\}$ *and* $\{r = r_2\}$ *are hyperbolic limit cycles of* X *with alternate stability. From* [FGG07]*, we can deduce that, for each limit cycle, the vector field*

$$Y_j := \begin{cases} \dot{r} &= r, \\ \dot{\theta} &= (b(r) - b(r_j))/(a(r)) \end{cases}$$

satisfies $[Y_j, X] = \mu\, Y_j$*, with* $\mu(r) = r\, a'(r)$*.*

Let us take now Y_1*. It is clear that, in general,* $\dot{\theta}$ *is not defined on* $r = r_2$ *since* $a(r_2) = 0$*. However, if* $b(r_2) = b(r_1)$ *(both limit cycles have the same period!), then* $\dot{\theta}$ *may be extended on* $r = r_2$ *and thus,* $\{r = r_2\}$ *may be contained in the domain* Ω *where the isochrons of* $\{r = r_1\}$ *are defined. This is the case, for instance, when the system is rigid (*$\dot{\theta}$ *=constant), for which the isochrons are straight lines from the origin.*

In the case that $b(r_2) \neq b(r_1)$ *(different periods like the numerical example illustrated in Fig. 6),* $\dot{\theta}$ *in* Y_1 *is not bounded close to* $\{r = r_2\}$ *and, then, the isochrons of* $\{r = r_1\}$ *spiral around.*

10. Discussion

An integrated way to study the dynamics around a limit cycle. We want to emphasize on the completeness of the method presented in this paper. We provide a way to reconcile different concepts, from Lie symmetries to phase resetting curves and surfaces, through the implementation of the parameterization method. Although computing PRSs has been presented as our last goal, along the way we

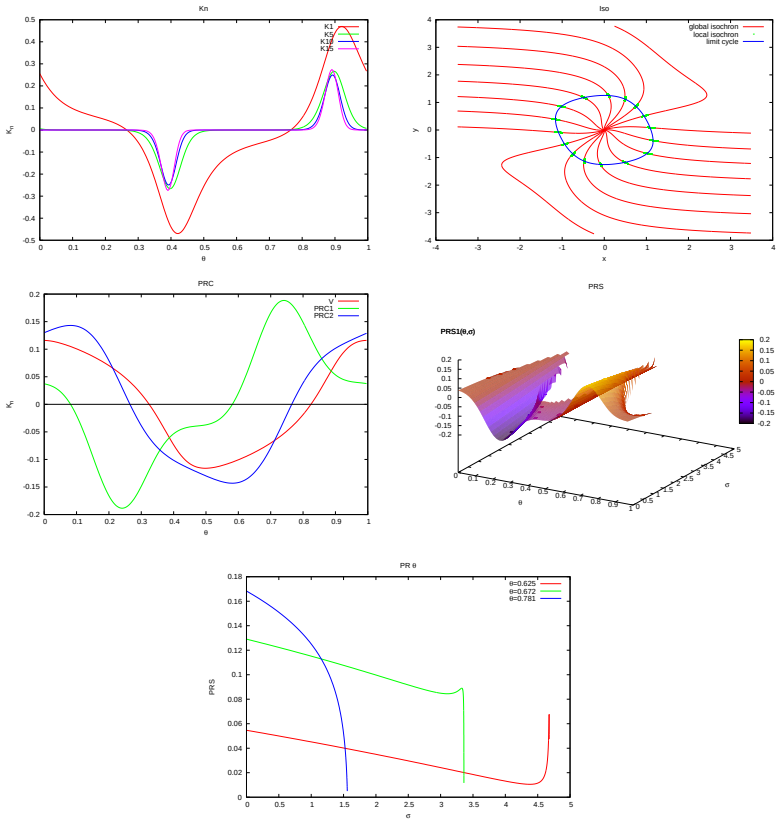

FIGURE 2. The van der Pol oscillator. In the panel PRC, we show PRC_1 and PRC_2 with amplitude 1 and x scaled by a factor 0.1. See Section 9.1.1 for a general explanation about the contents of each panel. In panel ($\mathtt{PR}\theta$), notice the diversity of phase advancements that can be obtained in the same isochron (three isochrons are shown: $\theta = 0.625, 0.672, 0.781$).

have related all the different concepts involved in the parameterization of a neighborhood of a periodic orbit in $\mathbb{R}^2$: choice of "canonical co-ordinates" inspired by the Lie symmetry, computation of isochrons, PRCs and, finally, PRSs. We have established, as well, a link between different parts of the scientific literature that are not usually connected: theoretical and numerical methods for invariant objects, qualitative theory of (mostly planar) ordinary differential equations and theoretical (neuro)biology.

We have also taken care of the numerical aspects involved in the method, which are not trivial and show up relationships among geometry, dynamics and numerical schemes. Concerning to the practical part of the effective computation, the above examples have shed light upon different biological and numerical issues that we would like to remark next.

From "Type 1" to "Type 2" PRCs. As we mentioned in the Introduction, from [Erm96], PRCs are classified between models with strictly positive or mainly positive PRC ("Type 1" or "Class 1"), and models whose PRC changes sign ("Type 2" or "Class 2"). The "rule of thumb" proposed by Ermentrout is that Type 1 PRC correspond to models in which oscillations appear via saddle-node

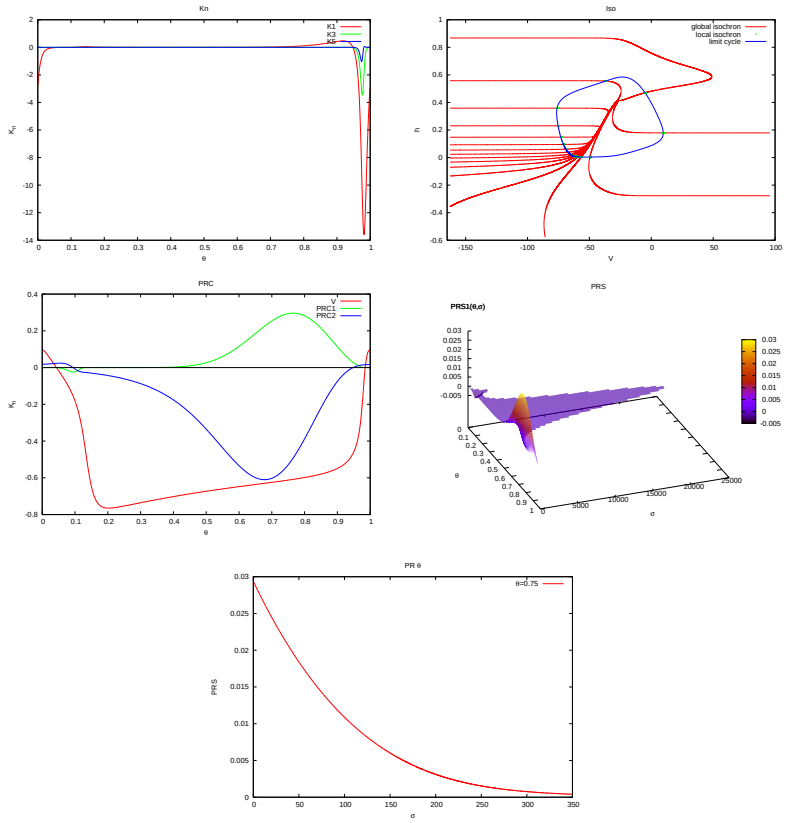

FIGURE 3. Two dimensional Hodgkin-Huxley close to a SNIC bifurcation. In the panel PRC, we show PRC_1 and PRC_2 with amplitude 10 and 0.1 respectively, and V scaled by a factor 0.01. See Section 9.1.1 for a general explanation about the contents of each panel. In panel (`Iso`), notice the heterogeneity in the distances between isochrons with equidistant phases, thus reflecting the slow-fast nature of the system.

on invariant circle bifurcations, whereas Type 2 PRC correspond to supercritical Andronov-Hopf bifurcation.

Our examples confirm this rough classification and we have used them to give an idea how the transition between the two PRC types takes place. Another study, using only PRCs and continuation methods, has recently appeared in [GS06].

Analytically, we have seen for instance (see Example 9.1) that $PRC_1(\theta) = -1/\sqrt{\beta}\sin(\theta)$ close to a Hopf bifurcation and (see Example 9.2), $PRC_1(\theta) = -\sin(\Omega(\theta))/(\sqrt{\beta}(m-\sin(\Omega(\theta)))$, where Ω is given in (38), for a system that presents a SNIC bifurcation at $m = 1$ (see also Fig. 1).

These examples clearly show that the fact that systems with oscillations coming from a saddle-node bifurcation are of "Type 1", that is, the PRC is mainly positive (or mainly negative), is produced by the slow-fast dynamics; moreover, the time it spends on a negative (resp., positive) regime is very short compared to the time it spends out of it. This fact can also be observed when comparing (40) with $I_{app} = 10$ (see Fig. (3)) with (40) with $I_{app} = 165$ (see Fig. (4)). For instance, in Fig. (3), panel (`PRC`), we can appreciate a small negative portion of the PRC_1 (close to $\theta = 0.1$), whereas in the same panel of Fig. (4), the negative part has a

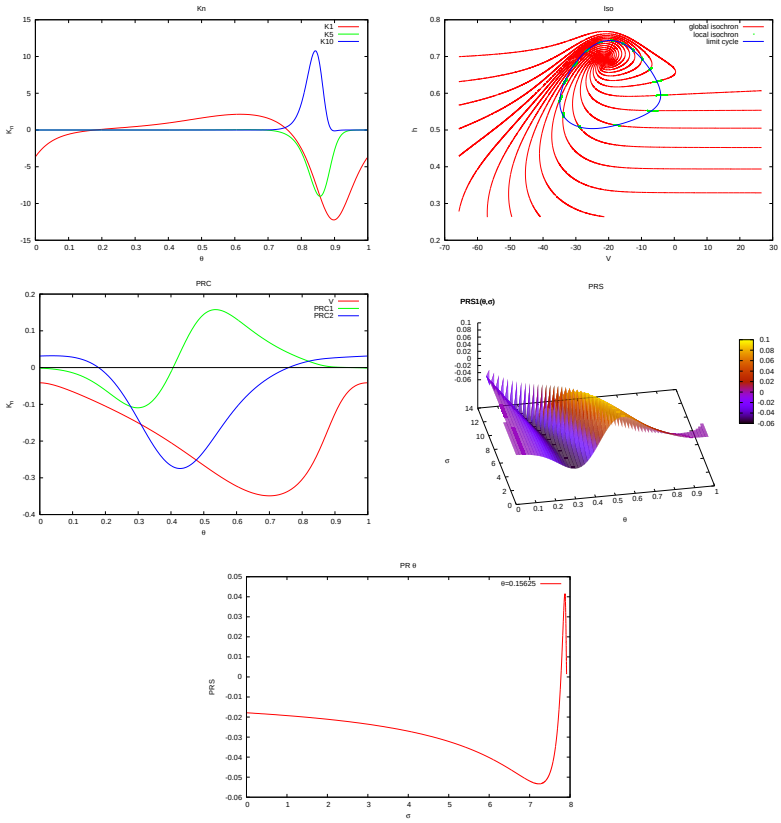

FIGURE 4. Two dimensional Hodgkin-Huxley close to a Hopf bifurcation. In the panel PRC, we show PRC_1 and PRC_2 with amplitude 2 and 0.02 respectively, and V scaled by a factor 0.01. See Section 9.1.1 for a general explanation about the contents of each panel.

bigger area. As the value I_{app} increases from $I_{app} = 10$ on, the negative portion of the PRC is enlarging up to the bifurcation point $I_{app} \approx 213.8$, where the PRC has practically zero integral.

Observe also that systems with a marked "Type II" tendency (mainly, (39), (40) with $I_{app} = 165$ or (41)) reach the extreme values of the PRCs when the isochrons have maximal curvature nearby the limit cycle (the correspondence is not exact because it also depends on the stimulus direction). Compare panels (`PRC`) with panels (`Iso`) in Figs. 2, 4 and 5. On the other hand, the chosen value for the Morris-Lecar system (see Fig. 6) shows an intermediate behavior, perhaps closer to "Type II" than to "Type I" (recall from (9.5) that it takes place close to a double limit cycle bifurcation).

Numerical drawbacks for slow-fast systems. From a joint analysis of panels (`Kn`) and (`Iso`) we can deduce the effect of slow versus fast dynamics. In Fig. 2, for instance, one can appreciate two features close to values $\theta \approx 0.4$ or $\theta \approx 0.9$: (a) the $K_n \neq 0$ for every n; (b) the isochrons on these zones are more separated (though the phases are equidistant). In other words, the slow dynamics makes the convergence of the Fourier expansions of our method to slow down as well. The numerical problem is that the value of K_n goes to zero faster in some zones, and it is then impossible to choose a uniform b (see Remark 7.2) such that the K_n can be

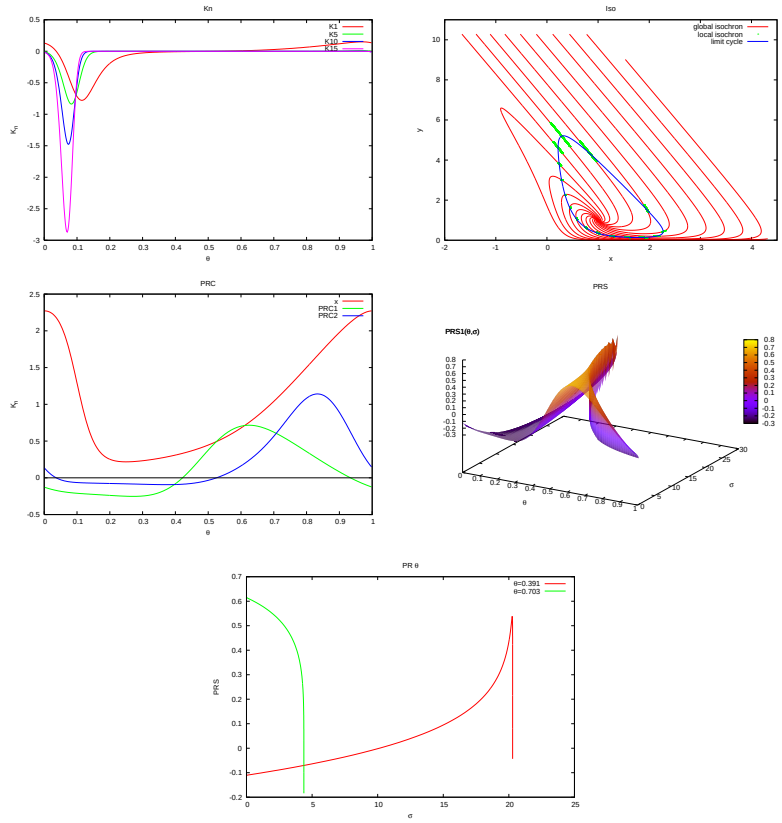

FIGURE 5. Selkov model with $a = 3$ and $b = 1$, not far from a Hopf bifurcation. See Section 9.1.1 for a general explanation about the contents of each panel.

kept to have order 1 for all the values of θ. Thus, for these values of θ, increasing the degree L of the Taylor polynomial does not have any effect in the growth of the domain where the isochron can be computed semi-analytically. This situation turns out to be a serious issue for the cases when the systems present an accentuated slow-fast dynamics.

This effect is even more dramatic in system (40) close to the SNIC bifurcation, see Fig. 3. In this case, (observe panel (`Kn`)) the zone close to $\theta = 0$, where the K_n take values orders of magnitude above the rest of the cycle; that is, $\dfrac{\max_\theta |K_n(\theta)|}{\min_\theta |K_n(\theta)|} \gg 1$. This coincides again with the zone where the isochrons are more noticeable separated, panel (`Iso`) of Fig. 3.

On the other hand, the factor $\dfrac{\max_\theta |K_n(\theta)|}{\min_\theta |K_n(\theta)|}$ is more attenuated in (40) close to the Hopf bifurcation, see Fig. 4.

Role of PRSs under high frequency stimulations. As explained in Section 1, the phase advancement computed on the limit cycle (PRC) can differ from that computed out of the limit cycle (PRS). This difference will be important under different circumstances like a short period of stimulation, a slow attraction to the limit cycle, a large stimulus amplitude, environmental random fluctuations, bursting-like stimuli, etc. We fix our attention, now, to panels (`PRS`) and (`PR`θ) in all the figures.

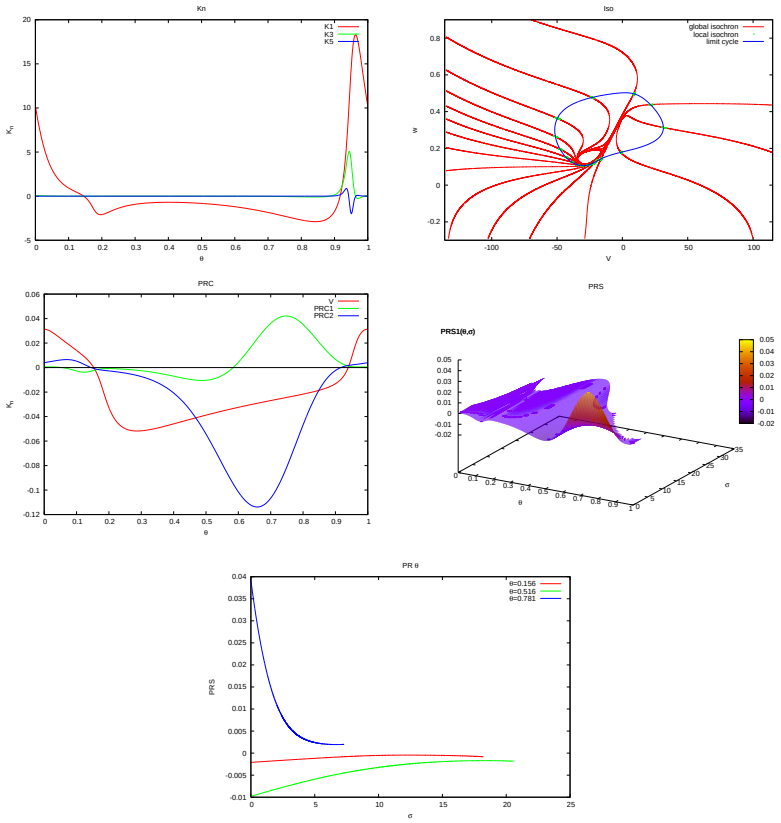

FIGURE 6. Morris-Lecar model. In the panel PRC, we show PRC_1 and PRC_2 with amplitude 1 and 0.01 respectively, and V scaled by a factor 0.001. See Section 9.1.1 for a general explanation about the contents of each panel. In panel (`Iso`), notice how isochrons spiral around the unstable limit cycle, see also Remark 9.5.

Our purpose is to highlight the differences in the phase advancement for points in a neighborhood of γ which share the same phase θ.

As with the maximum and minimum values of the PRCs, we pay attention to the zones where the curvature of the isochrons is extreme close to the limit cycle. This phenomenon can be timidly observed in Fig. 3, panel (`PR`θ), where the section $\theta = 0.75$ of the PRS is shown to be decreasing. More exaggerated variations can be obtained for $\theta = 0.15625$ in Fig. 4, panel (`PR`θ), or in Fig. 2. In the latter case, we show a *zoo* of possible sections ($\theta \in \{0.672, 0.625, 0.781\}$).

Changes of the phase advancement with respect to σ given a fixed θ, as the above examples show, combined with high frequency stimuli, rule out the possibility of controlling the whole phase advancement of an experiment using only the PRC. Thus, the PRSs become extremely useful. These differences, as our examples, show are more noticeable close to Type II oscillators (Hopf) because of the stronger curvature of the isochrons.

Our results agree with the fact that perturbations applied to Type II oscillators produce significant normal displacements from the limit cycle rather those applied to Type I. This fact has been also studied in [OC02] by Oprisan and Canavier, in the sense that the difference in angular velocity at displaced points compared to the angular velocity on the limit cycle is then more important. As pointed out in

[OC02], this might affect the study of biological circuits comprising Type II neural oscillators, which appear frequently in identified central pattern-generating circuits.

Isochrons in higher dimensions. Although in this paper we only apply the method to compute isochrons and PRCs to planar differential systems, it can be applied to higher dimensions provided that the limit cycle is hyperbolic and stable. In higher dimensions, we would like to emphasize the interesting question about the existence of an isochronous foliation when a limit cycle is not stable (i.e., some of the characteristic multipliers are bigger than one). In Section 8 we have shown that for a given vector field $X \in \mathbb{R}^n$, $n \geq 2$, with a limit cycle γ, if there exist $n-1$ non-trivial vector fields $Y_1, \ldots, Y_{n-1}$ in involution satisfying the Lie symmetry equation (4), then γ is isochronous and the foliation can be defined. An effective/efficient method to compute the isochrons for a limit cycle with both stable and unstable manifolds is also a challenge to which the Lie symmetries approach can help. We have seen in Section 8 that the problem of finding isochrons is equivalent to solving equation (35); that is, finding a 1-form ω_Y and a function λ satisfying $X(\omega_Y) = \lambda(\mathrm{x})\,\omega_Y$. The leaves of ω_Y will then be the isochronous sections of the limit cycle. Developing numerical methods to solve equation (35) would then give the isochronous sections, independently of the dimensions of the stable and unstable manifolds associated to the (hyperbolic) limit cycle. We want to emphasize, however, that this has more theoretical than practical interest since in models one usually encounters (hyperbolic) stable limit cycles. In this case, solving (35) would be equivalent to finding the stable manifold; the parameterization method could be useful as well, as in the bidimensional case.

Acknowledgments

The authors want to specially thank Rafael de la Llave for his guidance in the use of the parameterization methods. We are also very grateful to R. Calleja, A. Delshams, A. Jorba, A. Luque, P. Roldán, J. Villanueva and M. Zou with whom we have had fruitful discussions. This work has been partially supported by the MCyT/FEDER grant MTM2006-00478 (DACOBIA) and Generalitat de Catalunya grant number 2005SGR-986. G.H. has been also supported by the Spanish fellowship AP2003-3411 and the NSF Grant DMS 0354567.

References

[BHM04] E. Brown, P. Holmes, and J. Moehlis. On the phase reduction and response dynamics of neural oscillator populations. *Neural Comp.*, 16:673–715, 2004.

[CFL05] X. Cabré, E. Fontich, and R. de la Llave. The parameterization method for invariant manifolds. III. Overview and applications. *J. Differential Equations*, 218(2):444–515, 2005.

[CKWJ03] C. Cajochen, K. Kräuchi, and A. Wirz-Justice. Role of melatonin in the regulation of human circadian rhythms and sleep. *J. Neuroendocrinology*, 15:432–437, 2003.

[CL04] C. Chicone and W. Liu. Asymptotic phase revisited. *J. Differential Equations*, 204(1):227–246, 2004.

[DN94] A. Diez-Noguera. A functional model of the circadian system based on the degree of intercommunication in a complex system. *Am J Physiol Regul Integr Comp Physiol*, 267:R1118–R1135, 1994.

[EK91] G. B. Ermentrout and N. Kopell. Multiple pulse interactions and averaging in systems of coupled neural oscillators. *J. Math. Biol.*, 29(3):195–217, 1991.

[Erm96] G. B. Ermentrout. Type i membranes, phase resetting curves, and synchrony. *Neural Comp.*, 8:979–1001, 1996.

[Erm02] B. Ermentrout. *Simulating, analyzing, and animating dynamical systems*, volume 14 of *Software, Environments, and Tools*. Society for Industrial and Applied Mathematics (SIAM), Philadelphia, PA, 2002. A guide to XPPAUT for researchers and students.

[FGG07] E. Freire, A. Gasull, and A. Guillamon. Limit cycles and Lie symmetries. *Bull. Sci. Math.*, 131(6):501–517, 2007.

[Gri00] A. Griewank. *Evaluating derivatives*, volume 19 of *Frontiers in Applied Mathematics*. Society for Industrial and Applied Mathematics (SIAM), Philadelphia, PA, 2000. Principles and techniques of algorithmic differentiation.

[GS06] W. Govaerts and B. Sautois. Computation of the phase response curve: a direct numerical approach. *Neural Comput.*, 18(4):817–847, 2006.

[Guc75] J. Guckenheimer. Isochrons and phaseless sets. *J. Math. Biol.*, 1(3):259–273, 1974/75.

[HL06] À. Haro and R. de la Llave. A parameterization method for the computation of invariant tori and their whiskers in quasi-periodic maps: numerical algorithms. *Discrete Contin. Dyn. Syst. Ser. B*, 6(6):1261–1300 (electronic), 2006.

[Izh07] E. M. Izhikevich. *Dynamical systems in neuroscience: the geometry of excitability and bursting*. Computational Neuroscience. MIT Press, Cambridge, MA, 2007.

[JZ05] À. Jorba and M. Zou. A software package for the numerical integration of ODEs by means of high-order Taylor methods. *Experiment. Math.*, 14(1):99–117, 2005.

[KO98] B. Krauskopf and H. Osinga. Growing 1D and quasi-2D unstable manifolds of maps. *J. Comput. Phys.*, 146(1):404–419, 1998.

[ML81] C. Morris and H. Lecar. Voltage oscillations in the barnacle giant muscle fiber. *Biophys. J.*, 35:193–213, 1981.

[OC02] S. Oprisan and C. Canavier. The influence of limit cycle topology on the phase resetting curve. *Neural Comp.*, 14:1027–1057, 2002.

[Olv93] P. J. Olver. *Applications of Lie groups to differential equations*, volume 107 of *Graduate Texts in Mathematics*. Springer-Verlag, New York, second edition, 1993.

[PZG07] A.A. Ptitsyn, S. Zvonic, and J.M. Gimble. Digital signal processing reveals circadian baseline oscillation in majority of mammalian genes. *PLoS Comput Biol*, 3(6), 2007.

[RE98] J. Rinzel and G.B. Ermentrout. Analysis of neural excitability and oscillations. In C. Koch and I. Segev, editors, *Methods in Neural Modeling*, pages 135–169, Cambridge, MA, 1998. MIT Press.

[Sab05] M. Sabatini. Isochronous sections via normalizers. *Internat. J. Bifur. Chaos Appl. Sci. Engrg.*, 15(9):3031–3037, 2005.

[Sel68] E. Selkov. On the mechanism of single-frequency self-oscillations in glycolysis. a simple kinetic model. *Eur J Biochem*, 4:79–86, 1968.

[Sim90] C. Simó. On the analytical and numerical approximation of invariant manifolds. *Les Méthodes Modernes de la Méchanique Céleste, D. Benest and C. Froeschlé (eds.). Editions Frontières*, pages 285–329, 1990.

[Win75] A. T. Winfree. Patterns of phase compromise in biological cycles. *J. Math. Biol.*, 1(1):73–95, 1974/75.

Antoni Guillamon
Dept. de Matemàtica Aplicada I
Universitat Politècnica de Catalunya
Dr. Marañón 44-50, E-08028, Barcelona, Catalonia

E-mail address: antoni.guillamon@upc.edu

Gemma Huguet
Centre de Recerca Matemàtica
Apartat 50, E-08193, Bellaterra (Barcelona), Catalonia

E-mail address: gemma.huguet@upc.edu